BLANKET ENGINEERING

KEYWORDS: *neutronics integral experiment, full coverage blanket, beryllium*

NEUTRONICS INTEGRAL EXPERIMENTS OF SIMULATED FUSION REACTOR BLANKET WITH VARIOUS BERYLLIUM CONFIGURATIONS USING DEUTERIUM-TRITIUM NEUTRONS

CHIKARA KONNO, YUKIO OYAMA, YUJIRO IKEDA, SEIYA YAMAGUCHI, KOICHI TSUDA, KAZUAKI KOSAKO, HIROSHI MAEKAWA, MASAYUKI NAKAGAWA, TAKAMASA MORI, and TOMOO NAKAMURA *Japan Atomic Energy Research Institute*
Department of Reactor Engineering, Tokai Research Establishment
Tokai-mura, Naka-gun, Ibaraki-ken, 319-11 Japan

MOHAMED A. ABDOU *University of California, Los Angeles*
School of Engineering and Applied Science
Mechanical, Aerospace, and Nuclear Engineering Department
Los Angeles, California 90095

EDGAR F. BENNETT and KARL G. PORGES
Argonne National Laboratory, Fusion Power Program, Building 205
9700 South Cass Avenue, Argonne, Illinois 60439

MAHMOUD Z. YOUSSEF *University of California, Los Angeles*
School of Engineering and Applied Science
Mechanical, Aerospace, and Nuclear Engineering Department
Los Angeles, California 90095

Received September 29, 1994
Accepted for Publication March 29, 1995

Fusion neutronics experiments are performed on a full-coverage blanket with various configurations of a beryllium neutron multiplier. In the basic experimental system, a lithium carbonate enclosure contains a lithium oxide test zone and a deuterium-tritium neutron source to simulate a neutron spectrum in a fusion reactor. Five beryllium configurations are adopted to examine the effects of neutron multiplication and reflection by beryllium. The measurements are carried out along the central line in the test zone. Various measurement techniques are applied to obtain the tritium production rate distribution, which is one of the most important parameters for assessing the total tritium breeding ratio in a fusion blanket. In addition, the reaction rates and the neutron spectrum are measured to provide test data for confirmation of calculation results. These data are compared among six different configurations of the experimental system. Consistency between the different techniques for each measured parameter is also tested among different experimental systems. The experimental results are compared with the calculations by DOT 3.5 using JENDL-3/PR1 and /PR2. The calculation differs from the experimental data by <10%, except for the beryllium zone.

I. INTRODUCTION

Tritium fuel self-sufficiency is one of the key issues in the development of deuterium-tritium (D-T) fusion reactors. The accuracy of tritium breeding ratio estimation is required[1] to be within 2% in the fusion blanket design, although the blanket configuration of a fusion device is very complicated in terms of a three-dimensional torus shape and various component material structures (first wall, beryllium multiplier, coolant channel, etc.). The Japan Atomic Energy Research Institute (JAERI)/U.S. Department of Energy (U.S. DOE) collaborative program on fusion neutronics was began in 1984 at the Fusion Neutronics Source[2] (FNS) facility at JAERI to provide experimental data on neutronics parameters, e.g., tritium production rate (TPR), and to examine the prediction accuracy of the data. An open slab blanket assembly was used to perform the first-phase experiments[3,4] (Phase-I). The measurement technical basis was established[5,6] during this phase. The first series experimentally studied TPRs in lithium oxide (Li_2O) with/without a beryllium neutron multiplier. However, room-returned neutrons were proved to significantly affect TPR at the front regions of the blanket assembly.

The idea of completely surrounding the D-T neutron source by a blanket material was proposed to solve this room-returned neutron problem. The merit of this configuration was that it would simulate the neutron environment of a fusion device including the reflection components of the low-energy neutrons. Integral neutronics experiments that used this configuration were executed as the second phase[7] of the JAERI/U.S. DOE collaboration program. The basic experimental system consisted of a lithium carbonate (Li_2CO_3) enclosure and a Li_2O test zone. The Li_2CO_3 enclosure simulated the blanket except for the test blanket zone. The neutron source characterization experiment was performed before the current experiment to make the neutron source characterization inside the cavity clear. The results are reported separately.[7,8]

Various configurations of beryllium were adopted for the integral test of neutron multiplication performance because many designs use beryllium as a neutron multiplier. The effects of a closed system and a neutron multiplier of beryllium were examined in the first step (Phase-IIA). The experimental system in the second step (Phase-IIB) had a lined beryllium layer on the inner surface of the Li_2CO_3 enclosure. The D-T source was covered with not only breeding materials but also a neutron multiplier. Two different configurations of beryllium in the test blanket region were tested. These assemblies were used to study the effects of beryllium. The combined information from both the Phase-IIA and -IIB experiments provided the neutron multiplication effects of beryllium for these configurations studied.

The TPR, the activation reaction rate, and the neutron spectra were measured in the test blanket region. Because TPR is the data of primary interest, several measuring techniques were adopted to mitigate the systematic errors. The consistency among the various techniques was examined. Measured data obtained in the different experimental configurations were compared with each other to make the effects of beryllium clear. The experimental results were compared with calculations by the DOT3.5 code[9] using the JENDL-3/PR1 (Ref. 10) and /PR2 (Ref. 11) evaluated data libraries.

II. EXPERIMENTAL SETUP

II.A. Neutron Source

The experiments were performed in a room[2] 5 × 5 m wide and 4.5 m high at FNS. A water-cooled rotating tritium-titanium target was used to produce D-T neutrons via a $^3T(d,n)^4He$ reaction. The target disk rotated 800 rpm, and the head swung up and down to change the irradiated zone of the tritiated target. The point of neutron generation was at the center of the floor and 1.8 m high.

The deuteron beam energy and the current at the source position were 330 keV and 20 mA, respectively. The neutron yield was 3×10^{12} n/s at the initial condition of the tritiated target. The beam intensity was changed according to the neutron sensitivities of the measuring techniques.

The source neutron yield was absolutely determined by the associated alpha-particle counting technique.[12] The detector (the surface barrier semiconductor detector) for the associated alpha particles was set in the d^+ beam drift tube at a 178.4-deg angle. The associated alpha-particle method, however, could not be used for the high-current operation because of a longer dead time. In the case of heavy irradiation of more than 1 mA, ^{238}U and ^{232}Th fission counters, which were calibrated by the associated alpha-particle counting scheme at a low-flux level, were used as the external neutron monitor. The ^{238}U counter was located inside the experimental assembly, and the ^{232}Th counter was attached to the ceiling of the room just above the target location, as shown in Fig. 1.

II.B. Experimental Configurations

The key concept of the closed experimental system was introduced to isolate the room-returned neutrons and to adjust the neutron energy spectrum incident to the test blanket assembly to simulate the neutron environment of a fusion reactor. For this purpose, the neutron source point was enclosed by some materials similar to the blanket. Lithium carbonate was chosen as the enclosure (or container) because it is less costly than Li_2O. The basic geometry of this experimental system is shown in Fig. 1. The experimental system was constructed on a support table. The experiment was separated into two phases: Phases-IIA and -IIB.

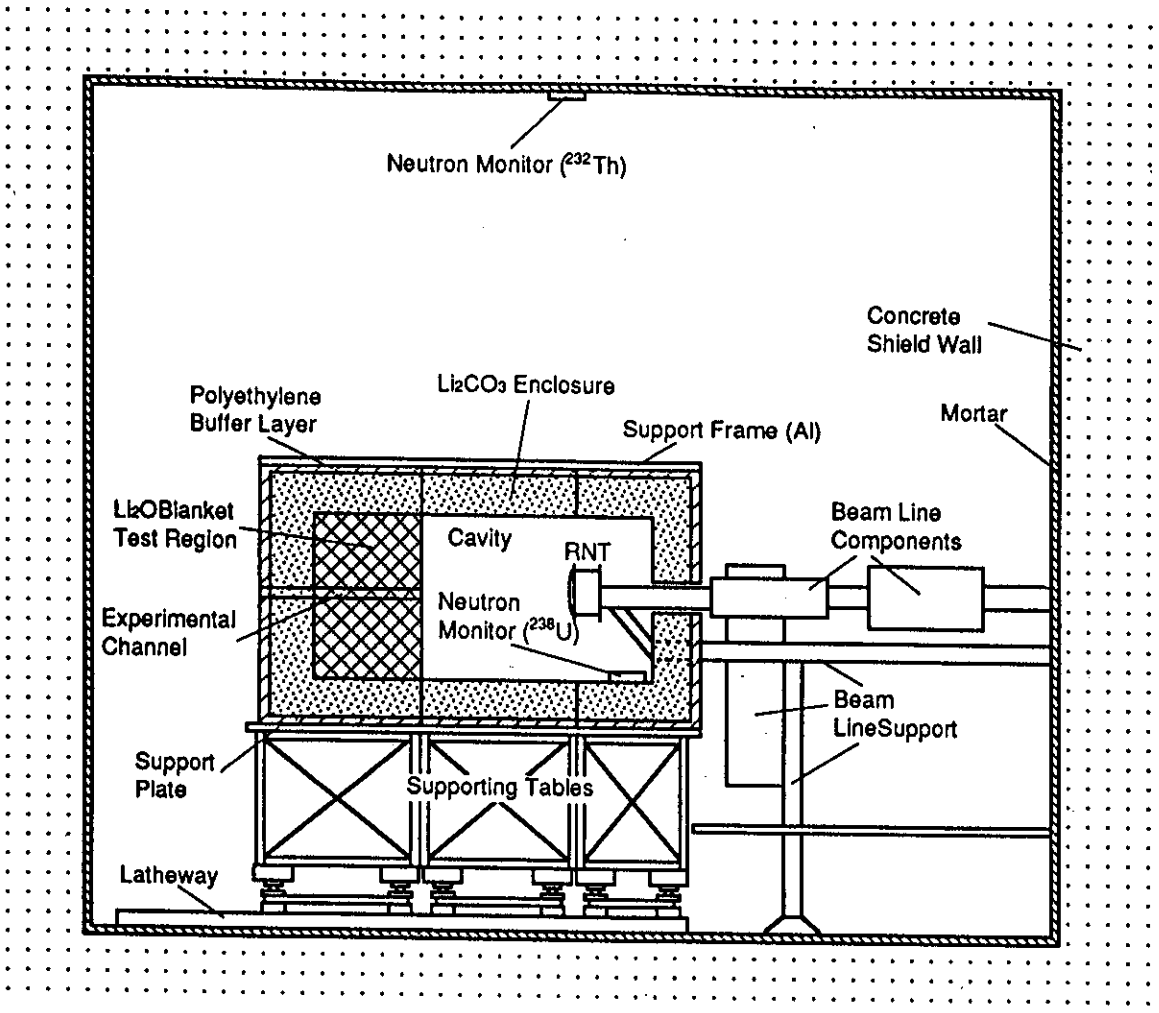

Fig. 1. Arrangement for the Phase-II experiment.

II.B.1. Phase-IIA System

Figure 2a shows the basic configuration of the experimental system called the reference (REF-A) blanket system in Phase-IIA. The dimensions given in Fig. 2a were used throughout all the experimental systems in both Phases-IIA and -IIB. The dimensions of the inner cavity were 870 × 870 × 1240 mm. The Li_2O test blanket region was 864 × 864 mm in face area and 607 mm in depth and was constructed by Li_2O blocks. The blocks consisted of cold-pressed natural Li_2O canned in a stainless steel box (made of Type 304 stainless steel and 50.6 mm square; 50.6, 101.2, or 202.4 mm long; and 0.2 mm thick). The density of Li_2O blocks was 75.5% of theoretical density, and the isotopic fraction of ^{6}Li was 7.41%. The neutron source point was set 780 mm from the test region surface. The cavity and the test region were enclosed by a 204 mm-thick Li_2CO_3 layer followed by a 50-mm-thick polyethylene layer for insulation of room-returned neutrons. The Li_2CO_3 zone was made of Li_2CO_3 bricks 51 × 101.5 × 203 mm^3, the surfaces of which were coated by an epoxy paint (0.1 mm) to prevent tritium release and moisture absorption. For the ceiling part of the cavity, the Li_2CO_3 bricks were suspended from the outer aluminum frame.

Measurements were performed in the Li_2O test blanket region. Four experimental channels, each with a cross section of 50.8 × 50.8 mm^2, were embedded in the test region for insertion of the detectors. The central and the off-central channels were set at the height of the central axis and 101.6 mm below the central axis along the axial direction, respectively. Two radial channels, namely, the front and the rear channels, were made at depths of 124 and 427.6 mm, respectively, from the front surface of the test region along the horizontal radial direction, perpendicular to the axial direction. The front and the rear channels were placed at heights 50.8 mm below and above the height of the central axis, respectively. Experimental drawers, which

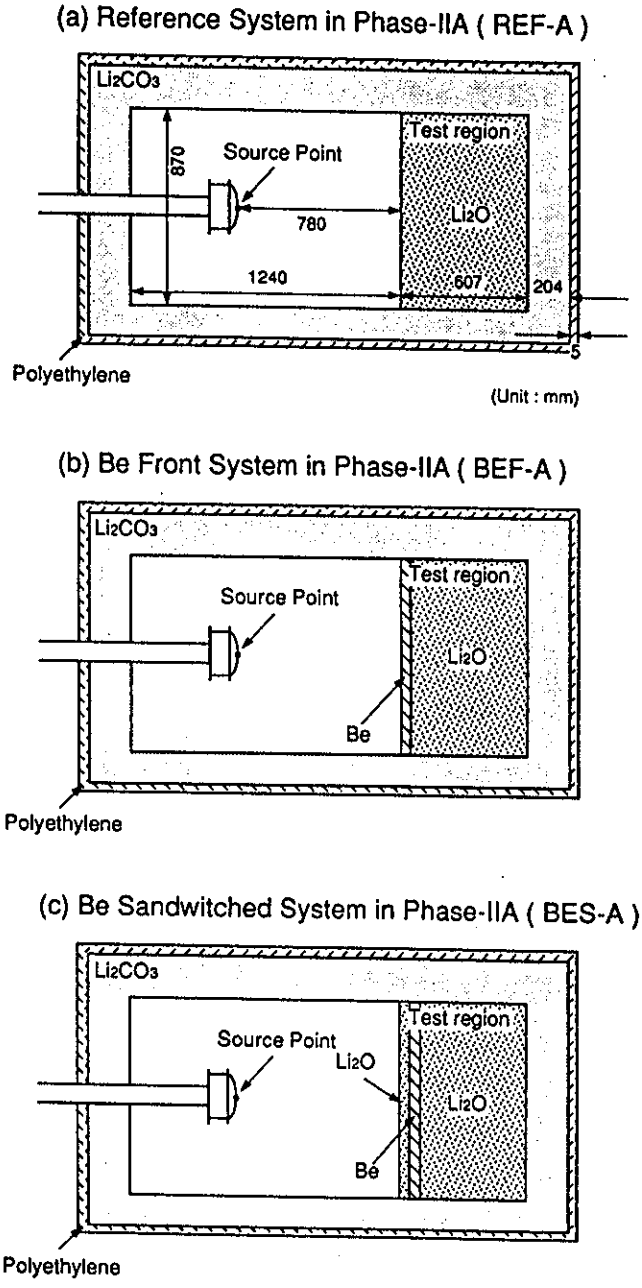

Fig. 2. Experimental configurations for (a) the reference (REF-A), (b) the beryllium front (BEF-A), and (c) the beryllium sandwiched (BES-A) blankets in Phase-IIA.

were stacked by the same materials as those in the same positions of the test region, were inserted into the channels with detectors.

Two material configurations with beryllium were also adopted in Phase-IIA to examine the effect of the neutron multiplication of beryllium. These configurations are illustrated in Fig. 2. These were a beryllium front system (BEF-A) with 50.8-mm-thick beryllium followed by 557-mm-thick Li_2O and a beryllium sandwiched system (BES-A) with 50.8-mm-thick Li_2O followed by 50.8-mm-thick beryllium and another Li_2O zone 507 mm long. Cubic beryllium bricks 50.8 × 50.8 × 50.8 mm^3 were used for the beryllium layer. The density of the beryllium bricks was 1.837 g/cm^3. The systems, BEF-A and BES-A, simulated the typical designs of the beryllium neutron multiplier arrangement.

II.B.2. Phase-IIB System

In the Phase-IIB system, 50.8-mm-thick beryllium and 5-mm-thick Type 304 stainless steel liners were added to the inner surface of the cavity of the Phase-IIA system to simulate beryllium tiles and the first wall, respectively, on the inboard blanket in a tokamak fusion reactor. The beryllium liner was expected to make the incident neutron spectrum in the test region much softer than that in the Phase-IIA system. The Type 304 stainless steel liner also played a role in supporting the beryllium liner. The size of the inner cavity (753 × 753 × 1178 mm) was somewhat smaller than that expected because there was additional space of a few millimetres between the beryllium and the Type 304 stainless steel. The distance from the neutron source to the test region surface and the size of the test blanket region were the same as those in Phase-IIA.

Three configurations in the test blanket region were tested: (a) the reference (only the Li_2O assembly, REF-B), (b) the beryllium front (a 50.8-mm-thick beryllium layer preceding the 557-mm-thick Li_2O assembly, BEF-B), and (c) the beryllium front system with a first wall of 5 mm-thick Type 304 stainless steel (BEFF-B). The cross-sectional views of these configurations are shown in Fig. 3. The configurations of REF-B and BEF-B were the same as those for REF-A and BEF-A, respectively. The configuration of BEFF-B was symmetrical with respect to the beryllium and Type 304 stainless steel liners in the cavity. The distance from the neutron source to the first wall of BEFF-B was 771 mm.

III. MEASUREMENTS

Because the D-T neutron source was surrounded by the Li_2CO_3 enclosure, the incident neutron flux into the test region included neutrons reflected by both the Li_2CO_3 and the target assembly structural materials. Therefore, examining the adequacy of the neutron source characteristics was very important. The neutron source characterization measurements were performed prior to the current measurements. These results are reported in Refs. 7 and 8. Based on the results in Refs. 7 and 8, we found that the calculation of the incident neutron spectrum agreed reasonably well with the measurement.

The current measurements were performed along the central axis in the test region. All measured data were given as per source neutron. The measurements

(a) Reference System in Phase-IIB (REF-B)

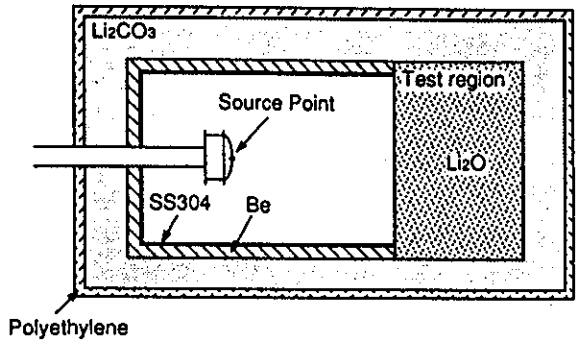

(b) Be Front System in Phase-IIB (BEF-B)

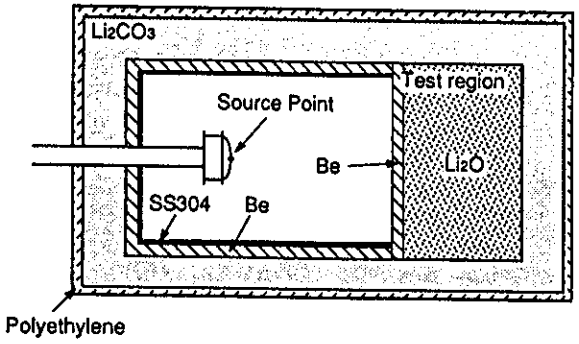

(c) Be Front with First Wall System in Phase-IIB (BEFF-B)

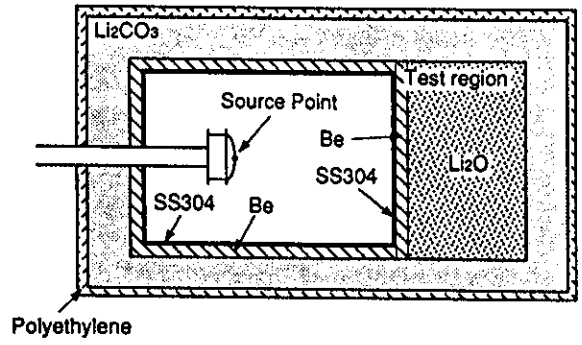

Fig. 3. Experimental configurations for (a) the reference (BEF-B), (b) the beryllium front (BEF-A), and (c) the beryllium front with first-wall (BEFF-B) blankets in Phase-IIB.

for each experimental configuration are summarized in Table I.

III.A. TPR

Several kinds of techniques have been applied to obtain TPR because it is a key nuclear parameter for a fusion reactor in assessing the total breeding ratio in a fusion blanket.

The TPR of ^{6}Li (T_6) was measured quickly by using the difference between the response of ^{6}Li-glass (^{6}Li: 96%) and that of ^{7}Li-glass (^{7}Li: ≥99.9%) in a mixed neutron-gamma radiation field.[5] Li-glasses with a diameter and thickness of 10 and 0.3 mm, respectively, were used to reduce the self-shielding effect in ^{6}Li-glass. A sharp peak caused by a ^{6}Li$(n,\alpha)^3$T reaction appeared on a Compton electron background produced by gamma rays in the pulse-height spectrum of ^{6}Li-glass. For ^{7}Li-glass, only the gamma-ray background was observed. Because one could assume that the gamma-ray responses of both scintillators would be almost identical, the gamma-ray background could be removed by subtracting the pulse-height spectrum of ^{7}Li-glass from that of ^{6}Li-glass. The total number of counts in the subtracted spectrum, which was equal to the total number of ^{6}Li$(n,\alpha)^3$T events in the scintillator, was proportional to TPR of ^{6}Li. The experimental error was 2 to 5%.

A Li-metal foil method[7] was adopted to measure TPRs of ^{6}Li (T_6) and ^{7}Li (T_7). Enriched ^{6}Li, ^{7}Li, and natural Li-metal samples were encapsulated in pure aluminum in a large glove box. The thickness of the metals was 0.5 mm to make the self-shielding effects smaller. The samples were exposed along the central axis. Tritium was extracted from the samples by furnace digestion in a carrier hydrogen atmosphere and converted to HTO on a hot copper oxide surface, whereas other techniques use lithium salt pellets from which HTO is extracted by wet chemistry procedures. Extracted tritium was measured by a low-background liquid scintillation counter system. The overall error was ~5%.

A new technique for T_6 and T_7 measurement, named the zonal method, has been developed.[7] The main principle of this method is to utilize the Li_2O bricks themselves as mass detectors while general conventional methods use small pellets placed between the stacked Li_2O blocks as detectors. The zonal method is expected to have the following advantages: (a) no perturbation of neutron flux by a detector, (b) large ratio of signal to background, and (c) mitigation of uncertainty due to the detector location, especially in the case where the gradient of the TPR distribution is very steep, e.g., the boundary of beryllium and Li_2O. Moreover, the zonal method gives proper benchmark data for Monte Carlo calculation because zonal experimental data can be directly compared with the calculation result of estimators of large volume such as track length estimators. The sintered type of Li_2O plates with a size of 13 × 48 × 48 mm and the cold-pressed plates with a size of 16 × 48 × 48 mm were used as mass detectors. These plates were canned in a stainless steel (Type 304 stainless steel) box like the Li_2O bricks. Natural Li_2O and enriched $^7Li_2O$ plates were irradiated. The irradiated plates were heated at a temperature of 650°C for 2 h. Tritium in the extracted gas was oxygenated to be measured by a liquid scintillation counting system. The TPR of ^{6}Li was deduced from both measured TPRs of

TABLE I

Measured Parameters

	TPR				Reaction Rate	Neutron Spcetrum		
	Li-Glass	Li-Metal	Zonal	NE-213	Activation Foil	NE-213	H_2-PRC	H_2/Kr-PRC
Phase-IIA								
Reference blanket (REF-A)	○[a]	○	○	○	○	○	○	×[b]
Beryllium front blanket (BEF-A)	○	×	×	○	×	○	○	○
Beryllium sandwiched blanket (BES-A)	○	○	○	○	○	○	○	×
Phase-IIB								
Reference blanket (REF-B)	○	×	×	○	×	○	×	×
Beryllium front blanket (BEF-B)	○	×	×	○	×	○	×	×
Beryllium front with first-wall blanket (BEFF-B)	○	○	○	○	○	○	○	○

[a]The symbol ○ designates measured.
[b]The symbol × designates not measured.

natural lithium (T_n) and ^{7}Li. The overall experimental error was ~3%.

The T_7 was indirectly derived by using the neutron spectrum above 2 MeV measured by a small sphere NE-213 scintillation spectrometer.[6] The threshold energy of the ^{7}Li$(n,n'\alpha)^3$T reaction (~3 MeV) was larger than the lower limit energy (2 MeV) of the measured neutron spectrum by NE-213. The T_7 was obtained by multiplying the measured neutron spectrum and the cross-section data of the ^{7}Li$(n,n'\alpha)^3$T reaction. The cross-section data for ^{7}Li$(n,n'\alpha)^3$T in JENDL-3/PR2 (Ref. 11) were used. The errors in the obtained T_7 were associated with the errors of the measured neutron flux spectrum and the cross-section data. The overall error was 6 to 10%.

The on-line TPR measurements, i.e., the Li-glass and the NE-213 methods, were applied to all cases. Those results gave the relative change in TPR among various configurations. The other techniques, the Li-foil and the zonal methods, needed heavy irradiation of neutrons for 10 h, so the configurations applied by them were limited in number to minimize activation of the experimental system and radiation hazard for the experimentalists.

III.B. Reaction Rate

The reaction rates for ^{27}Al$(n,\alpha)^{24}$Na, ^{58}Ni$(n,2n)^{57}$Ni, ^{58}Ni$(n,p)^{58}$Co, ^{93}Nb$(n,2n)^{92m}$Nb, ^{115}In$(n,n')^{115m}$In, and ^{197}Au$(n,\gamma)^{198}$Au were measured by the foil activation technique. These reaction rates served as the standard set of the neutron indices because the threshold energy of the reaction was scattered appropriately, as shown in Fig. 4. The relative change in the neutron flux distribution could be observed by comparing the reaction rate distributions in the different systems. The foils were 10 mm in diameter and 1 mm in thickness for aluminum, nickel, niobium, and indium. For gold, a 1-μm-thick foil was used to minimize the self-shielding effect. The foils were put into a narrow space between the Li_2O bricks in the test regions along the central axis and were irradiated with D-T neutrons for ~10 h, the source strength of which was ~2 to 3 × 10^{12}/s. After irradiation, the gamma rays emitted from the activated foils were measured by germanium detectors. The reaction rates were deduced from the measured activation rates. The experimental error ranged from 3 to 5%.

III.C. In-System Neutron Spectrum

A 14 mm-diam spherical NE-213 liquid scintillator[6] was used to measure the fast neutron spectrum in the system. The rise-time discrimination technique was used for the neutron gamma-ray separation. A gain stabilizer was adopted to avoid a gain drift of the system due to the counting rate variation or temperature change. Pulse-height spectra were unfolded by the FORIST code.[14] The response matrix was calculated by a Monte Carlo method,[6] which agreed with the measured response matrix within 5% (particularly within 2% at ~14 MeV). Because the neutron flux from 2 to 10 MeV was only one-tenth of that above 10 MeV, even a 2% error of the response matrix above 10 MeV might cause a large error of the neutron spectrum from 2 to 10 MeV. The overall experimental errors were 4% for the flux above 10 MeV and 10 to 20% for the flux from 2 to 10 MeV.

Neutron spectra from a few kilo-electron-volts to 1 MeV were measured by using a small-sized proton-recoil gas proportional counter[7,15] (PRC). Because PRC had a cylindrical shape whose outer diameter and sensitive length were 19 and 127 mm, respectively, PRC was inserted into the test region using two radial drawers with a small preamplifier, perpendicularly to the

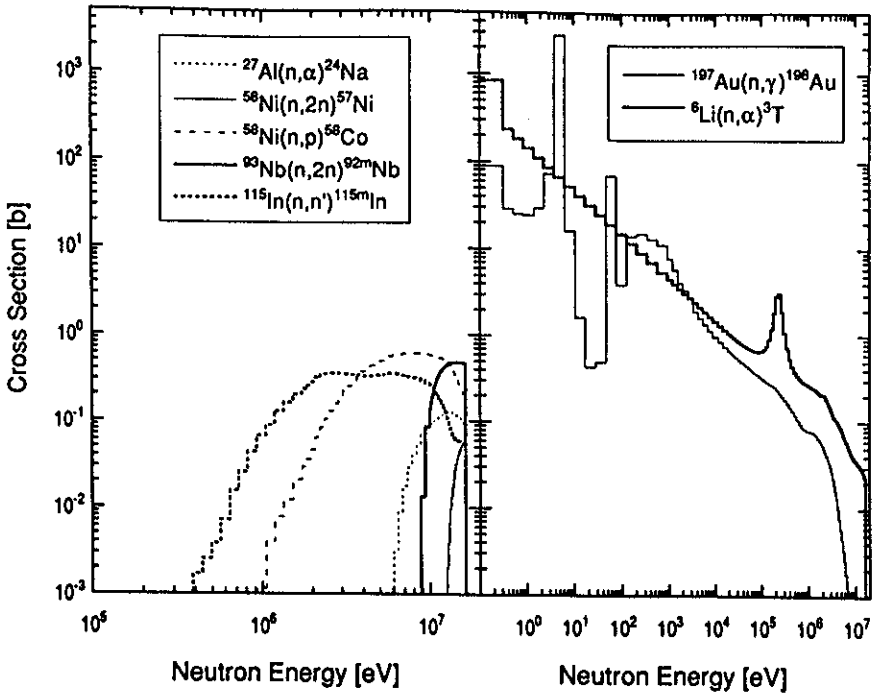

Fig. 4. The cross-section curves of $^{27}Al(n,\alpha)^{24}Na$, $^{58}Ni(n,2n)^{57}Ni$, $^{58}Ni(n,p)^{58}Co$, $^{93}Nb(n,2n)^{92m}Nb$, $^{115}In(n,n')^{115m}In$, $^{197}Au(n,\gamma)^{198}Au$, and $^{6}Li(n,\alpha)^{3}T$. The data of the 125-group structure converted from the JENDL-3 dosimetry file[13] are shown.

direction of the central axis of the system. Horizontal uniformity of the neutron flux was assumed. To encompass the neutron spectrum over the energy range from a few kilo-electron-volts to 1 MeV, two different gas fillings were used for otherwise identical counters: hydrogen at 5.5 atm with 1% CH_4 for the low-energy component (a few kilo-electron-volts to 150 keV) and a 50-50 mixture of hydrogen and krypton at 8.8 atm for the upper energy component (150 keV to 1 MeV). Krypton increased the stopping power, thereby reducing the range of recoil protons in the counter. Neutron and gamma-ray events were discriminated by the difference of the rise time. Neutron spectra were obtained by differentiating recoil proton spectra. The total error was 3 to 10% above 10 keV. The neutron spectrum below 10 keV tended to become smaller because of the uncertainty of the W value, which was the average energy lost by the incident particle per ion pair formed.

IV. RESULTS AND DISCUSSION

IV.A. Experimental Results

IV.A.1. Phase-IIA System

The measured TPRs in all the assemblies including the Phase-IIB assemblies are summarized in Tables II through V. The TPR of ^{6}Li measured by Li-glass and Li-metal was not corrected for self-shielding and neutron perturbation by the detector void, the effects of which were large only in the beryllium zone, as described in Sec. IV.B. Figure 5 shows the TPR distributions of ^{6}Li (T_6) along the central axis, measured by Li-glass and Li-metal. The enhancement at the front of the test region in the reference blanket (REF-A) was attributed to the low-energy neutrons reflected in the cavity. Large peaks at the center of the beryllium layer appeared in the beryllium front (BEF-A) and the beryllium sandwiched (BES-A) blankets. Room-returned neutrons from the back side increased T_6 at the end of Li_2CO_3. Note that this effect disappeared in the Li_2O test region. The TPR distributions of ^{7}Li (T_7) by NE-213 are shown in Fig. 6. The T_7 distributions for REF-A, BEF-A, and BES-A were very similar to each other, although T_7 was slightly smaller behind the beryllium layer in BEF-A and BES-A. The TPR distributions of natural lithium (T_n) measured by the zonal method are plotted in Fig. 7. No data in the beryllium layer are available. The increase of TPR by the beryllium layer in BES-A is attributed for the increase of T_6 by the neutron multiplication effect of beryllium in spite of the small abundance (7.41%) of ^{6}Li in natural lithium.

The measured reaction rates for $^{27}Al(n,\alpha)^{24}Na$, $^{58}Ni(n,2n)^{57}Ni$, $^{58}Ni(n,p)^{58}Co$, $^{93}Nb(n,2n)^{92m}Nb$, $^{115}In(n,n')^{115m}In$, and $^{197}Au(n,\gamma)^{198}Au$ are summarized in Tables VI and VII. Figure 8 shows the measured reaction rate distributions along the central axis in REF-A and BES-A. The gradients of the reaction rate distributions reflected their threshold energy. The trend of

TABLE II

Measured TPR of ^{6}Li by Li-Glass

Distance from Neutron Source (mm)	Reference Blanket (REF-A)	Beryllium Front Blanket (BEF-A)	Beryllium Sandwiched Blanket (BES-A)
Phase-IIA			
778.9	(9.52 ± 0.95)E−29[a]	(3.00 ± 0.10)E−28	(1.38 ± 0.05)E−28
804.2	(7.94 ± 0.48)E−29	(4.74 ± 0.14)E−28	(1.55 ± 0.06)E−28
827.0			(2.44 ± 0.08)E−28
829.5		(2.91 ± 0.10)E−28	(2.54 ± 0.09)E−28
842.1	(6.45 ± 0.47)E−29	(1.81 ± 0.06)E−28	
854.8		(1.36 ± 0.05)E−28	(4.22 ± 0.14)E−28
880.1		(1.00 ± 0.04)E−28	
892.6	(5.66 ± 0.29)E−29		(2.64 ± 0.09)E−28
894.1			
905.4			(1.58 ± 0.05)E−28
930.7			(1.23 ± 0.04)E−28
981.3		(7.09 ± 0.25)E−29	(8.95 ± 0.32)E−29
		(5.30 ± 0.20)E−29	(6.05 ± 0.27)E−29
993.8	(4.09 ± 0.21)E−29		
1082.5		(3.32 ± 0.14)E−29	
1095.0	(2.80 ± 1.41)E−29		(3.52 ± 0.13)E−29
1183.7		(2.12 ± 0.07)E−29	
1196.2	(1.84 ± 0.08)E−29		(2.11 ± 0.09)E−29
1284.9	(1.29 ± 0.06)E−29	(1.31 ± 0.05)E−29	(1.31 ± 0.05)E−29
1386.1	(1.06 ± 0.04)E−29	(1.10 ± 0.04)E−29	(1.07 ± 0.04)E−29
1487.7	(8.50 ± 0.30)E−30	(9.68 ± 0.34)E−30	(8.56 ± 0.29)E−30
1538.5	(1.06 ± 0.04)E−29		
1589.3	(5.68 ± 0.18)E−29	(5.12 ± 0.14)E−29	(5.10 ± 0.14)E−29
Phase-IIB			
Distance from Neutron Source (mm)	Reference Blanket (REF-B)	Beryllium Front Blanket (BEF-B)	Beryllium Front with First-Wall Blanket (BEFF-B)
780.4	(1.98 ± 0.07)E−27	(5.29 ± 0.19)E−27	(4.73 ± 0.16)E−27
793.0	(6.11 ± 0.21)E−28		
805.7	(3.63 ± 0.13)E−28	(4.06 ± 0.16)E−27	(4.04 ± 0.15)E−27
831.0	(2.28 ± 0.09)E−28	(1.72 ± 0.06)E−27	(1.67 ± 0.06)E−27
843.6		(4.55 ± 0.16)E−28	(4.49 ± 0.16)E−28
856.3		(2.76 ± 0.10)E−28	(2.67 ± 0.09)E−28
881.6	(1.37 ± 0.05)E−28	(1.71 ± 0.06)E−28	(1.63 ± 0.06)E−28
932.2	(5.66 ± 0.19)E−29		(1.01 ± 0.03)E−28
979.8		(7.69 ± 0.27)E−29	(7.36 ± 0.24)E−29
982.8	(7.28 ± 0.25)E−29		
1081.0			(4.14 ± 0.14)E−29
1084.0	(4.33 ± 0.15)E−29		
1182.2		(2.48 ± 0.08)E−29	
1185.2	(2.57 ± 0.08)E−29		(2.34 ± 0.08)E−29
1283.4			(1.37 ± 0.05)E−29
1286.4	(1.56 ± 0.05)E−29		
1384.6		(1.21 ± 0.04)E−29	(1.10 ± 0.04)E−29
1387.6	(1.27 ± 0.04)E−29		
1486.2			(8.46 ± 0.28)E−30
1489.2	(9.56 ± 0.32)E−30		
1587.8		(4.72 ± 0.13)E−29	
1590.8	(5.17 ± 0.14)E−29		(4.30 ± 0.14)E−29

[a]Read as (9.52 ± 0.95) × 10^{-29} (per source neutron per lithium).

TABLE III

Measured TPR of ^{6}Li and ^{7}Li by Li-Metal

Distance from Neutron Source (mm)	Phase-IIA				Phase-IIB	
	Reference Blanket (REF-A)		Beryllium Sandwiched Blanket (BES-A)		Beryllium Front with First-Wall Blanket (BEFF-B)	
	TPR of ^{6}Li	TPR of ^{7}Li	TPR of ^{6}Li	TPR ^{7}Li	TPR of ^{6}Li	TPR of ^{7}Li
780.2	(9.77 ± 0.49)E−29[a]	(6.37 ± 0.32)E−30	(1.11 ± 0.06)E−28	(6.56 ± 0.33)E−30	(5.66 ± 0.28)E−27	(7.35 ± 0.37)E−30
805.5	(8.18 ± 0.41)E−29	(5.67 ± 0.28)E−30	(2.01 ± 0.10)E−28	(5.67 ± 0.28)E−30	(4.56 ± 0.23)E−27	(6.20 ± 0.31)E−30
818.1					(3.73 ± 0.19)E−27	(5.44 ± 0.27)E−30
830.8	(7.10 ± 0.36)E−29	(4.94 ± 0.25)E−30	(2.80 ± 0.14)E−28	(5.08 ± 0.25)E−30	(1.65 ± 0.08)E−27	(4.90 ± 0.25)E−30
843.4					(4.54 ± 0.23)E−28	(4.45 ± 0.22)E−30
856.1	(6.94 ± 0.35)E−29	(4.23 ± 0.21)E−30	(4.40 ± 0.22)E−28	(5.62 ± 0.28)E−30	(2.83 ± 0.14)E−28	(3.94 ± 0.20)E−30
868.7					(2.18 ± 0.11)E−28	(3.54 ± 0.18)E−30
881.4			(2.39 ± 0.12)E−28	(3.98 ± 0.20)E−30	(1.80 ± 0.09)E−28	(3.16 ± 0.16)E−30
906.7			(1.16 ± 0.06)E−28	(2.93 ± 0.15)E−30		
932.0	(5.01 ± 0.25)E−29	(2.61 ± 0.13)E−30	(8.90 ± 0.45)E−29	(2.39 ± 0.12)E−30		
1033.2	(3.62 ± 0.18)E−29	(1.23 ± 0.06)E−30	(4.48 ± 0.22)E−29	(1.11 ± 0.06)E−30	(1.26 ± 0.06)E−28	(2.02 ± 0.10)E−30
1134.4	(2.50 ± 0.13)E−29	(5.44 ± 0.27)E−30	(2.43 ± 0.12)E−29	(4.75 ± 0.24)E−31	(5.53 ± 0.28)E−29	(9.28 ± 0.46)E−31
1235.6	(1.68 ± 0.08)E−29	(2.51 ± 0.13)E−31	(1.87 ± 0.09)E−29	(2.06 ± 0.10)E−31	(3.19 ± 0.16)E−29	(4.31 ± 0.22)E−31
1336.8	(1.17 ± 0.06)E−29	(1.29 ± 0.06)E−31	(1.06 ± 0.05)E−29	(1.05 ± 0.05)E−31	(1.87 ± 0.09)E−29	(2.00 ± 0.10)E−31
1387.4	(1.09 ± 0.05)E−29	(7.92 ± 0.40)E−32			(1.14 ± 0.06)E−29	(9.50 ± 0.48)E−32
1438.0	(1.10 ± 0.06)E−29	(5.67 ± 0.28)E−32	(1.06 ± 0.05)E−29	(4.70 ± 0.24)E−32		

[a]Read as (9.77 ± 0.49) × 10^{-29} (per source neutron per lithium).

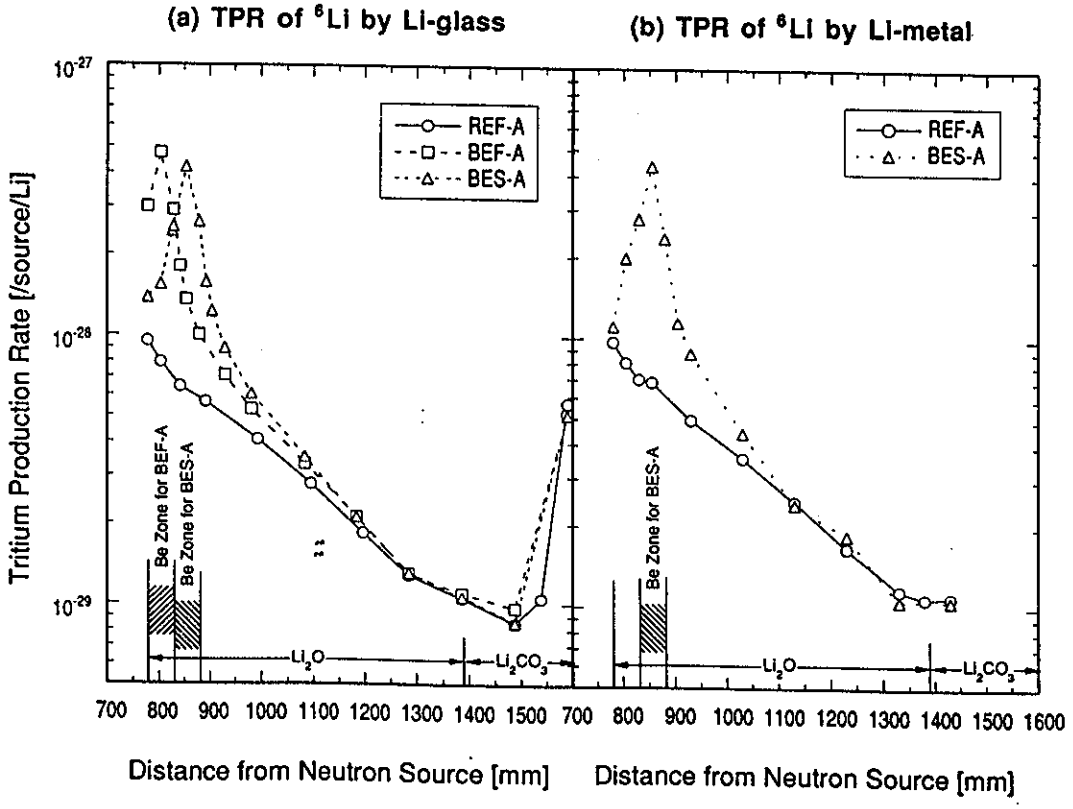

Fig. 5. Measured ^{6}Li TPRs by (a) Li-glass scintillator and (b) Li-metal in Phase-IIA.

TABLE IV

Measured TPR by Zonal Method

Distance from Neutron Source (mm)	TPR of ^{nat}Li	TPR of ^{7}Li	TPR of ^{6}Li
Reference Blanket (REF-A) in Phase-IIA			
777.7 to 800.7	(1.19 ± 0.06)E−29[a]	(6.16 ± 0.10)E−30	(8.28 ± 0.41)E−29
800.7 to 823.7	(1.06 ± 0.05)E−29		
823.7 to 846.7	(9.26 ± 0.46)E−30		
846.7 to 869.7	(8.45 ± 0.42)E−30	(4.17 ± 0.10)E−30	(6.08 ± 0.30)E−29
869.7 to 892.7	(7.58 ± 0.38)E−30		
892.7 to 915.7	(6.82 ± 0.34)E−30		
915.7 to 938.7	(6.31 ± 0.32)E−30	(2.62 ± 0.04)E−30	(5.14 ± 0.26)E−29
938.7 to 973.6	(5.43 ± 0.27)E−30		
980.0 to 1029.1	(4.37 ± 0.22)E−30		
1029.1 to 1078.2	(3.44 ± 0.17)E−30	(1.09 ± 0.04)E−30	(3.22 ± 0.16)E−29
1078.2 to 1127.3	(2.61 ± 0.13)E−30		
1127.3 to 1176.4	(2.07 ± 0.10)E−30		
1182.8 to 1231.9	(1.59 ± 0.08)E−30	(3.39 ± 0.04)E−31	(1.69 ± 0.08)E−29
1231.9 to 1281.0	(1.21 ± 0.06)E−30		
1281.0 to 1330.1	(9.64 ± 0.48)E−31		
1330.1 to 1379.2	(8.29 ± 0.42)E−31	(1.01 ± 0.07)E−31	(9.75 ± 0.49)E−30
Beryllium Sandwiched Blanket (BES-A) in Phase-IIA			
778.2 to 790.8	(1.56 ± 0.08)E−29	(6.03 ± 0.30)E−30	(1.33 ± 0.07)E−28
790.8 to 803.4	(1.59 ± 0.08)E−29		
803.4 to 813.0	(1.64 ± 0.08)E−29		
813.0 to 825.6	(1.94 ± 0.10)E−29	(5.40 ± 0.27)E−30	(1.91 ± 0.10)E−28
876.0 to 888.8	(1.70 ± 0.09)E−29	(3.43 ± 0.17)E−30	(1.83 ± 0.09)E−28
888.8 to 901.6	(1.26 ± 0.06)E−29		
901.6 to 914.4	(1.07 ± 0.05)E−29		
914.4 to 927.2	(9.11 ± 0.46)E−30	(2.56 ± 0.13)E−30	(8.93 ± 0.45)E−29
927.2 to 937.0	(8.03 ± 0.40)E−30		
937.0 to 949.8	(7.49 ± 0.38)E−30		
949.8 to 959.6	(6.83 ± 0.34)E−30	(1.89 ± 0.09)E−30[b]	(6.44 ± 0.32)E−29[b]
959.6 to 972.4	(6.34 ± 0.32)E−30		
977.7 to 1026.7	(5.16 ± 0.26)E−30		
1026.7 to 1075.7	(3.80 ± 0.19)E−30	(9.65 ± 0.48)E−31	(3.86 ± 0.19)E−29
1075.7 to 1124.7	(2.99 ± 0.15)E−30		
1124.7 to 1173.7	(2.27 ± 0.11)E−30		
1180.4 to 1229.4	(1.67 ± 0.08)E−30	(2.86 ± 0.14)E−31	(1.86 ± 0.09)E−29
1229.4 to 1278.4	(1.29 ± 0.06)E−30		
1278.4 to 1327.4	(9.91 ± 0.50)E−31		
1327.4 to 1376.4	(8.22 ± 0.41)E−31	(9.02 ± 0.45)E−32	(9.78 ± 0.49)E−30
Beryllium Front with First-Wall Blanket (BEFF-B) in Phase-IIB			
777.7 to 790.6	(6.43 ± 0.32)E−29	(5.57 ± 0.28)E−30	
790.6 to 803.5	(2.86 ± 0.14)E−29	(4.79 ± 0.24)E−30	
803.5 to 816.4	(2.12 ± 0.11)E−29	(4.21 ± 0.21)E−30	
816.4 to 826.4	(1.75 ± 0.09)E−29	(3.80 ± 0.19)E−30	
826.4 to 842.2	(1.46 ± 0.07)E−29		
842.2 to 855.0	(1.26 ± 0.06)E−29		
855.0 to 867.8	(1.15 ± 0.06)E−29		
867.8 to 877.5	(1.05 ± 0. 5)E−29		
931.6 to 980.5	(5.50 ± 0.28)E−30	(1.33 ± 0.07)E−30	
1084.8 to 1134.2	(2.28 ± 0.11)E−30	(4.31 ± 0.22)E−30	
1238.4 to 1287.2	(9.51 ± 0.48)E−31		

[a]Read as (1.19 ± 0.06) × 10^{-29} (per source neutron per lithium).
[b]Region of this sample is from 949.6 to 972.2 mm.

TABLE V

Measured TPR of ^{7}Li by NE-213

Phase-IIA			
Distance from Neutron Source (mm)	Reference Blanket (REF-A)	Beryllium Front Blanket (BEF-A)	Beryllium Sandwiched Blanket (BES-A)
730.20	(5.50 ± 0.56)E−30[a]	(5.41 ± 0.55)E−30	(5.39 ± 0.45)E−30
791.70	(5.20 ± 0.51)E−30	(5.24 ± 0.49)E−30	(5.45 ± 0.50)E−30
817.00	(4.74 ± 0.42)E−30	(4.57 ± 0.40)E−30	(4.84 ± 0.44)E−30
842.30		(3.85 ± 0.32)E−30	(4.03 ± 0.34)E−30
854.80	(3.84 ± 0.33)E−30		
867.60			(3.38 ± 0.28)E−30
892.90		(2.82 ± 0.24)E−30	(2.78 ± 0.23)E−30
905.40	(2.75 ± 0.22)E−30		
994.10		(1.35 ± 0.10)E−30	(1.34 ± 0.11)E−30
1006.6	(1.33 ± 0.09)E−30		
1095.3		(6.38 ± 0.55)E−31	(6.14 ± 0.40)E−31
1107.8	(6.05 ± 0.43)E−31		
1196.5		(2.70 ± 0.18)E−31	(2.69 ± 0.19)E−31
1209.0	(2.69 ± 0.19)E−31		
1297.7	(1.30 ± 0.08)E−31	(1.17 ± 0.07)E−31	(1.18 ± 0.08)E−31
1395.9	(5.73 ± 0.36)E−32		
1398.9		(5.09 ± 0.34)E−32	(5.09 ± 0.36)E−32
1500.1		(2.09 ± 0.14)E−32	(2.12 ± 0.15)E−32
1500.5	(2.34 ± 0.15)E−32		
1601.3		(7.84 ± 0.61)E−33	(7.95 ± 0.56)E−33
1602.1	(8.97 ± 0.60)E−33		

Phase-IIB			
Distance from Neutron Source (mm)	Reference Blanket (REF-B)	Beryllium Front Blanket (BEF-B)	Beryllium Front with First-Wall Blanket (BEFF-B)
730.20	(5.98 ± 0.61)E−30	(5.92 ± 0.53)E−30	(5.92 ± 0.53)E−30
791.70	(5.66 ± 0.58)E−30	(6.00 ± 0.43)E−30	(5.65 ± 0.49)E−30
817.00		(5.24 ± 0.46)E−30	(4.36 ± 0.34)E−30
842.30	(4.45 ± 0.41)E−30	(4.40 ± 0.36)E−30	(4.00 ± 0.32)E−30
892.90	(3.22 ± 0.28)E−30	(3.17 ± 0.24)E−30	(2.87 ± 0.22)E−30
994.10	(1.58 ± 0.13)E−30	(1.50 ± 0.12)E−30	(1.36 ± 0.97)E−30
1095.3	(7.34 ± 0.57)E−31		(6.00 ± 0.38)E−31
1196.5	(3.35 ± 0.29)E−31	(3.00 ± 0.20)E−31	(2.66 ± 0.17)E−31
1297.7	(1.41 ± 0.11)E−31		(1.15 ± 0.07)E−31
1398.9	(6.10 ± 0.48)E−32	(5.52 ± 0.36)E−32	(5.01 ± 0.31)E−32
1500.1	(2.60 ± 0.19)E−32	(2.35 ± 0.15)E−32	(2.07 ± 0.13)E−32
1601.3	(9.97 ± 0.78)E−33	(8.59 ± 0.53)E−33	(7.76 ± 0.53)E−33

[a]Read as $(5.50 \pm 0.56) \times 10^{-30}$ (per source neutron per lithium).

the reaction rate distributions for the threshold reactions was almost the same between the two systems, as observed in the T_7 distribution. On the other hand, the reaction rates of the $^{197}Au(n,\gamma)^{198}Au$ reaction were quite different in the vicinity of the beryllium layer. The distribution of $^{197}Au(n,\gamma)^{198}Au$ showed almost the same trend as that of T_6 because the shape of the cross section was almost similar except for the resonance, as shown in Fig. 4. The effect of different blanket materials was clearly observed at the boundary of Li_2O and Li_2CO_3, and the effect of the room-returned neutrons appeared only at the rear of the Li_2CO_3 zone.

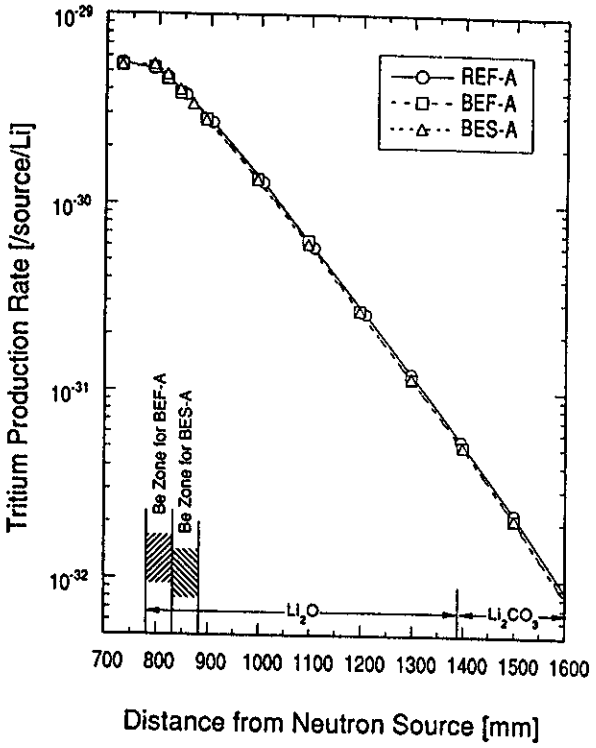

Fig. 6. Measured ^{7}Li TPRs by NE-213 scintillator in Phase-IIA.

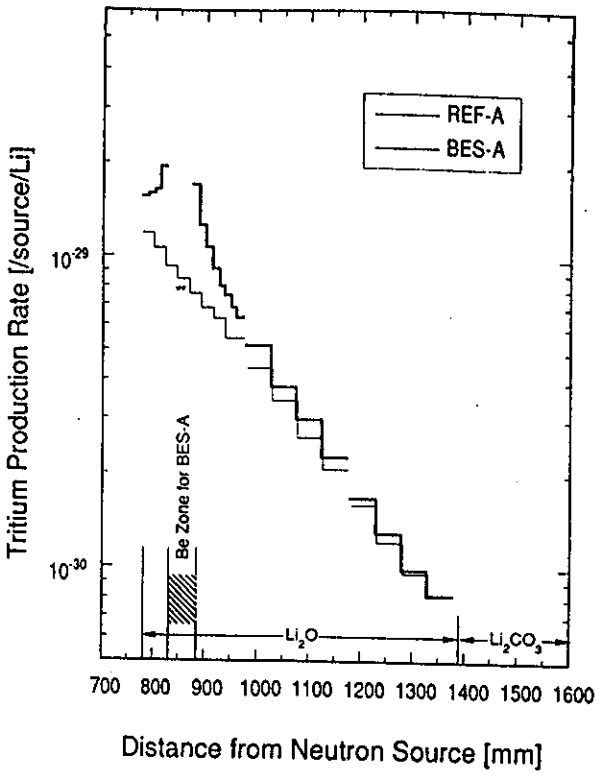

Fig. 7. Measured ^{nat}Li TPRs by zonal method in Phase-IIA.

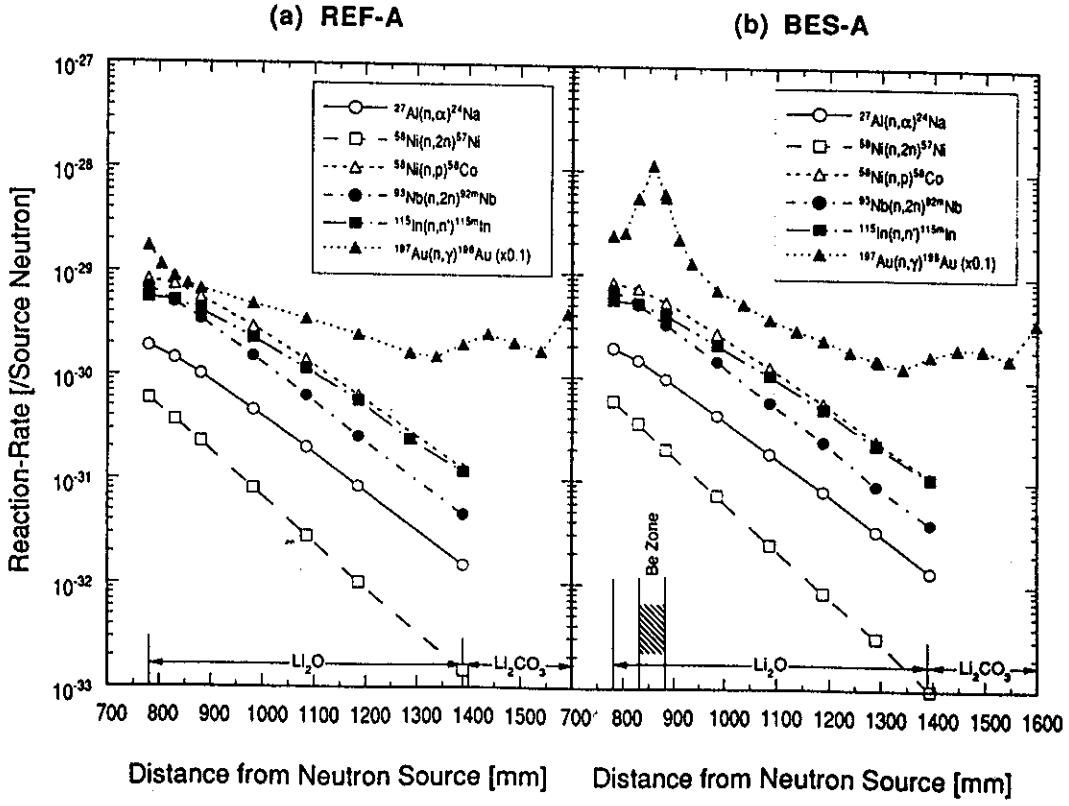

Fig. 8. Measured activation reaction rates for (a) the reference and (b) the beryllium sandwiched (BES-A) blankets in Phase-IIA.

TABLE VI

Measured Reaction Rates for the Reference (REF-A) Blanket in Phase-IIA

Distance from Neutron Source (mm)	$^{27}Al(n,\alpha)^{24}Na$	$^{58}Ni(n,2n)^{57}Ni$	$^{58}Ni(n,p)^{58}Co$	$^{93}Nb(n,2n)^{92m}Nb$	$^{115}In(n,n')^{115m}In$	$^{197}Au(n,\gamma)^{198}Au$
780.2	1.903E−30(2.7)[a]	5.882E−31(2.8)	8.200E−30(2.7)	6.943E−30(2.7)	5.545E−30(2.7)	1.719E−28(2.7)
805.5						1.142E−28(3.0)
831.0	1.456E−30(2.8)	3.684E−31(2.9)	7.417E−30(2.8)	4.982E−30(2.6)	5.186E−30(2.7)	8.814E−29(3.3)
856.3						7.561E−29(3.3)
881.7	1.033E−30(2.8)	2.292E−31(2.9)	5.579E−30(2.9)	3.459E−30(2.8)	4.153E−30(2.7)	6.754E−29(3.0)
983.4	4.621E−31(2.8)	8.089E−32(2.8)	2.923E−30(2.8)	1.521E−30(2.8)	2.277E−30(2.7)	4.813E−29(3.1)
1084.7	2.024E−31(2.9)	2.826E−32(3.0)	1.407E−30(2.9)	6.378E−31(2.8)	1.162E−30(2.8)	3.484E−29(3.1)
1186.4	8.575E−32(2.9)	1.011E−32(3.2)	6.471E−31(2.8)	2.589E−31(2.8)	5.722E−31(2.8)	2.496E−29(3.0)
1287.1						1.680E−29(3.1)
1337.9						1.548E−29(3.0)
1389.5	1.514E−32(3.4)	1.459E−33(6.7)	1.308E−31(3.2)	4.668E−32(2.7)	1.23E−31(4.0)	2.040E−29(3.1)
1437.2						2.569E−29(3.2)
1488.2					5.12E−32(4.1)	2.122E−29(3.2)
1539.7						1.769E−29(2.9)
1591.1					2.04E−32(11)	4.045E−29(3.0)
1642.0					1.68E−32(17)	6.814E−29(3.3)

[a]Read as 1.903×10^{-30} (per source neutron) with 2.7% relative error.

TABLE VII

Measured Reaction Rates for the Beryllium Sandwiched (BES-A) Blanket in Phase-IIA

Distance from Neutron Source (mm)	$^{27}Al(n,\alpha)^{24}Na$	$^{58}Ni(n,2n)^{57}Ni$	$^{58}Ni(n,p)^{58}Co$	$^{93}Nb(n,2n)^{92m}Nb$	$^{115}In(n,n')^{115m}In$	$^{197}Au(n,\gamma)^{198}Au$
780.2	1.944E−30(2.6)[a]	5.914E−31(2.7)	8.304E−30(2.6)	7.140E−30(2.6)	5.636E−30(2.6)	2.341E−29(2.9)
803.2						2.511E−29(2.8)
828.5	1.491E−30(2.7)	3.645E−31(3.1)	7.341E−30(2.8)	5.160E−30(2.7)	5.278E−30(2.6)	5.428E−29(2.9)
830.8						5.432E−29(2.8)
858.6						1.139E−28(2.6)
881.7						6.055E−29(2.7)
884.0	9.944E−31(2.7)	2.047E−31(3.2)	5.468E−30(2.8)	3.320E−30(2.7)	4.088E−30(2.8)	5.565E−29(2.8)
909.5						2.213E−29(2.9)
934.4						1.310E−29(3.0)
985.5	4.443E−31(2.8)	7.390E−32(3.4)	2.756E−30(2.8)	1.490E−30(2.7)	2.158E−30(2.7)	7.248E−30(3.1)
1036.4						5.339E−30(3.2)
1087.2	1.923E−31(2.9)	2.495E−32(3.6)	1.321E−30(2.8)	6.040E−31(2.8)	1.101E−30(2.7)	3.850E−30(3.2)
1137.7						3.013E−30(3.3)
1188.5	8.304E−32(2.9)	8.631E−33(3.8)	5.944E−31(3.0)	2.530E−31(2.9)	5.187E−31(2.8)	2.447E−30(3.3)
1239.5						1.887E−30(3.3)
1289.9	3.425E−32(3.5)	3.176E−33(4.9)	2.584E−31(2.9)	9.450E−32(2.8)	2.343E−31(3.1)	1.597E−30(3.3)
1294.2						1.521E−30(3.4)
1341.0						1.339E−30(3.4)
1394.5	1.366E−32(4.2)	1.001E−33(5.2)	1.152E−31(3.4)	4.020E−32(3.1)	1.097E−31(3.7)	1.756E−30(3.2)
1446.0						2.056E−30(2.8)
1494.7						2.041E−30(3.3)
1545.7						1.654E−30(3.0)
1596.8						3.644E−30(3.0)

[a]Read as 1.944×10^{-30} (per source neutron) with 2.6% relative error.

The measured in-system neutron spectra for BEF-A are shown in Fig. 9 along with the spectra calculated with DOT3.5 (Ref. 9), which is described in Sec. VI.E. The spectra above 2 MeV were measured by NE-213 while those from a few kilo-electron-volts to 1 MeV were measured by PRC. The large dip at 260 keV due to the resonance of the $^6Li(n,\alpha)^3T$ reaction and the small dips at 440 and 1000 keV due to the resonance of the $^{16}O(n,n)$ reaction clearly appear in Fig. 9.

IV.A.2. Phase-IIB System

All the measuring techniques were applied to the beryllium front with the first-wall blanket (BEFF-B). The on-line methods (NE-213 and Li-glass) were used in all three blanket configurations to examine the effects of the first wall and beryllium on TPR. Figure 10 shows the TPR distributions of ^6Li (T_6) measured by Li-glass along the central axis. The enhancement at the front of the test region in the reference blanket (REF-B) was much larger than that in the reference blanket (REF-A) in Phase-IIA because the beryllium liner in the cavity produced more low-energy neutrons. The beryllium layer at the front of the test region also enhanced T_6 more in the beryllium front (BEF-B) and the beryllium front with the first-wall (BEFF-B) blankets. The increase of T_6 at the end of the Li_2CO_3 zone in Fig. 10 is attributed to room-returned neutrons from the backward direction, as described in the Phase-IIA systems. The first wall in BEFF-B slightly decreased T_6 just behind the first wall. Figure 11 shows the TPR distributions of ^7Li (T_7) by NE-213. The distributions for REF-B, BEF-B, and BEFF-B are almost the same, although T_7 in BEFF-B is smaller behind the beryllium layer.

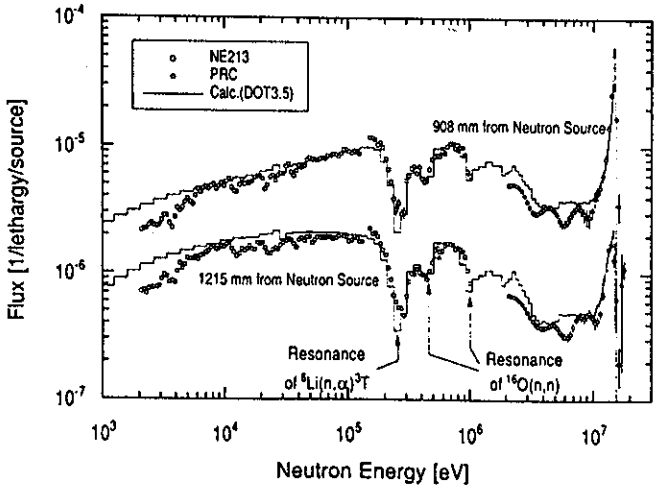

Fig. 9. Measured and calculated neutron spectra 908 and 1215 mm from the neutron source for the beryllium front (BEF-A) blanket in Phase-IIA.

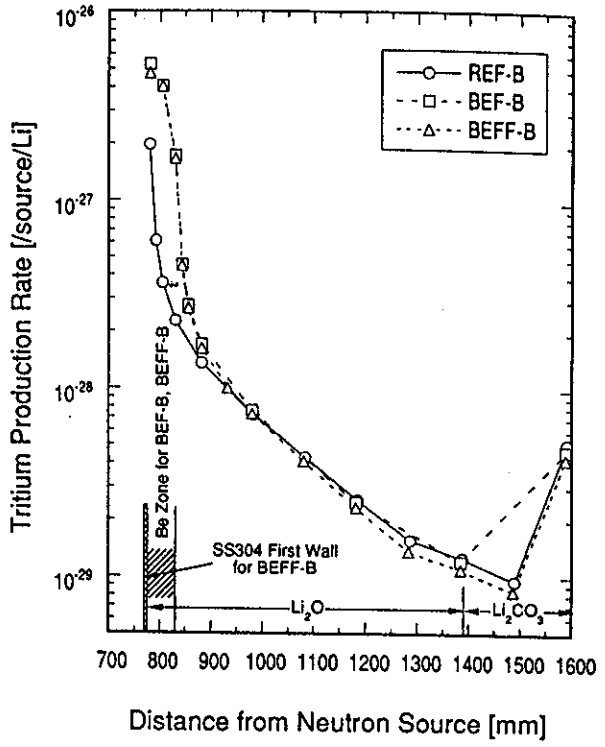

Fig. 10. Measured ^6Li TPRs by Li-glass scintillator in Phase-IIB.

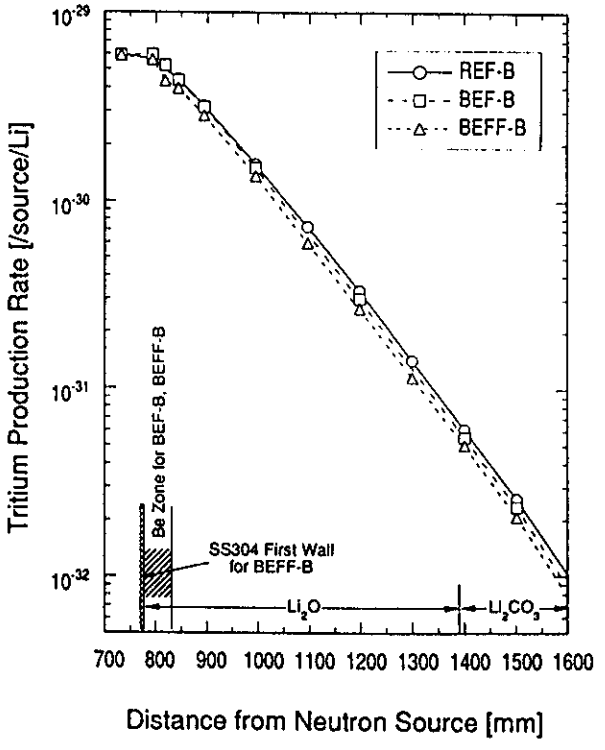

Fig. 11. Measured ^7Li TPRs by NE-213 scintillator in Phase-IIB.

The reaction rates for $^{27}Al(n,\alpha)^{24}Na$, $^{58}Ni(n,2n)^{57}Ni$, $^{58}Ni(n,p)^{58}Co$, $^{93}Nb(n,2n)^{92m}Nb$, $^{115}In(n,n')^{115m}In$, and $^{197}Au(n,\gamma)^{198}Au$ were measured only in the beryllium front with the first-wall (BEFF-B) blanket. The measured reaction rates are summarized in Table VIII and shown in Fig. 12. The reaction rate distributions of the threshold reactions were similar to the reference (REF-A) and the beryllium sandwiched (BES-A) blankets in Phase-IIA. The effect of the beryllium liner in the cavity and the beryllium layer in the test region appeared in the reaction rate distribution of the non-threshold reaction $^{197}Au(n,\gamma)^{198}Au$, as observed in T_6.

IV.B. Estimation of Flux Perturbation by Li-Glass and Li-Metal

A flux depression for the low-energy neutrons was caused by the detectors themselves such as Li-glass and Li-metal because enriched ^6Li was included in these detectors and the $^6Li(n,\alpha)T$ reaction had a huge resonance of ~260 keV. This is called the self-shielding effect. In the case of the Li-glass detector, neutron perturbation also occurred by a void for inserting the Li-glass, light guide, photomultiplier tube (PMT), and signal cable. The neutron flux distortion by the enriched ^6Li and a detector void was considered to be very large, particularly in the beryllium zone where the soft neutron spectra were encountered.

The effect of flux perturbation (self-shielding and detector void) on TPR of ^6Li (T_6) measured by Li-glass inside the beryllium layer was estimated[16] for the beryllium sandwiched blanket (BES-A) in Phase-IIA by using the DOT5.1 code[17] and the MATXS6 nuclear data set.[18] The Li-glass scintillator, the light guide, and PMT (PMT, ~10% aluminum) contained in the outer aluminum tube were modeled in the *r-z* two dimensions. Because the calculated T_6 with Li-glass was smaller by ~50% than that calculated in the model without the detector void and the Li-glass itself, T_6 measured by Li-glass inside the beryllium was considered to be different from the true T_6. On the other hand, according to the similar analysis, neglecting details of the Li-glass scintillator inside the Li_2O zone resulted in only an ~2% change in T_6.

TABLE VIII

Measured Reaction Rates for the Beryllium Front with First-Wall (BEFF-B) Blanket in Phase-IIB

Distance from Neutron Source (mm)	$^{27}Al(n,\alpha)^{24}Na$	$^{58}Ni(n,2n)^{57}Ni$	$^{58}Ni(n,p)^{58}Co$	$^{93}Nb(n,2n)^{92m}Nb$	$^{115}In(n,n')^{115m}In$	$^{197}Au(n,\gamma)^{198}Au$
774.2	1.942E−30(2.8)[a]	6.150E−31(2.9)	8.700E−30(2.7)	7.170E−30(2.7)	6.870E−30(2.8)	8.210E−28(2.6)
779.2	1.884E−30(2.8)	5.670E−31(2.9)	8.540E−30(2.8)	6.740E−30(2.8)	6.844E−30(2.8)	7.720E−28(2.7)
813.2						6.370E−28(2.7)
838.2	1.295E−30(2.8)	3.140E−31(3.2)	7.130E−30(2.7)	4.460E−30(2.8)	5.560E−30(2.7)	2.596E−28(2.7)
864.5						7.300E−29(2.7)
890.2	9.020E−31(2.9)	1.953E−31(3.4)	5.220E−30(2.8)	3.010E−30(2.7)	4.170E−30(2.8)	3.650E−29(2.8)
941.4						1.487E−29(2.8)
991.8	4.020E−31(2.9)	7.040E−32(3.6)	2.686E−30(2.8)	1.309E−30(2.8)	2.180E−30(2.8)	8.920E−30(2.9)
1042.8						6.780E−30(2.9)
1093.6	1.740E−31(2.9)	2.332E−32(3.6)	1.213E−30(2.7)	5.390E−31(2.8)	1.060E−30(2.8)	4.980E−30(3.0)
1144.7						4.040E−30(3.0)
1195.2	7.120E−32(3.1)	8.500E−33(3.6)	5.540E−31(2.8)	2.157E−31(2.8)	5.060E−31(2.9)	2.915E−30(3.2)
1246.3						2.460E−30(3.3)
1297.3	2.970E−32(3.1)	2.960E−33(4.3)	2.415E−31(2.8)	8.620E−32(2.8)	2.290E−31(3.0)	1.838E−30(2.8)
1348.4						1.699E−30(2.7)
1374.3						1.533E−30(2.7)
1398.4	1.241E−32(3.1)	1.029E−33(4.5)	1.081E−31(3.2)	3.594E−32(3.0)	1.191E−31(3.1)	2.014E−30(3.2)
1419.8						2.540E−30(3.1)
1445.7						2.335E−30(2.7)
1495.4						1.864E−30(3.2)
1546.9						1.645E−30(3.1)
1572.9						1.774E−30(2.7)
1599.0						3.370E−30(3.2)
1623.4						7.350E−30(3.0)
1647.9						4.840E−30(2.8)

[a]Read as 1.942×10^{-30} (per source neutron) with 2.8% relative error.

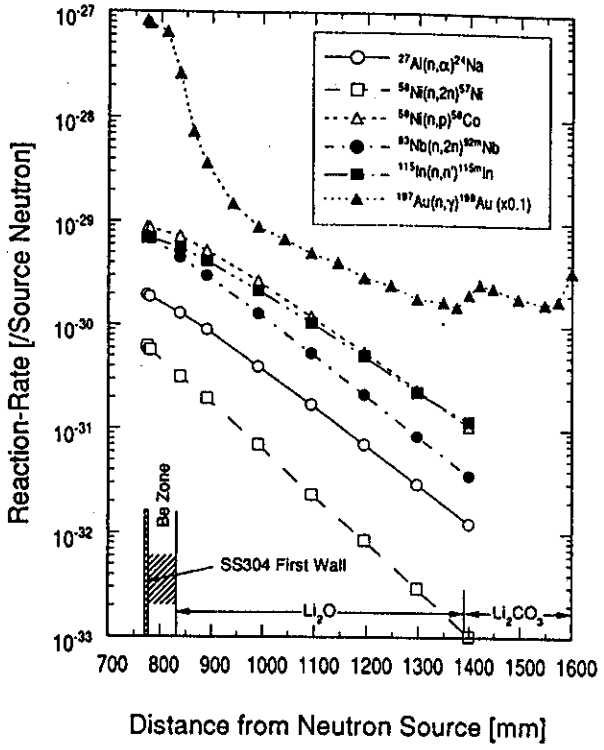

Fig. 12. Measured activation reaction rates for the beryllium front with first-wall (BEFF-B) blanket in Phase-IIB.

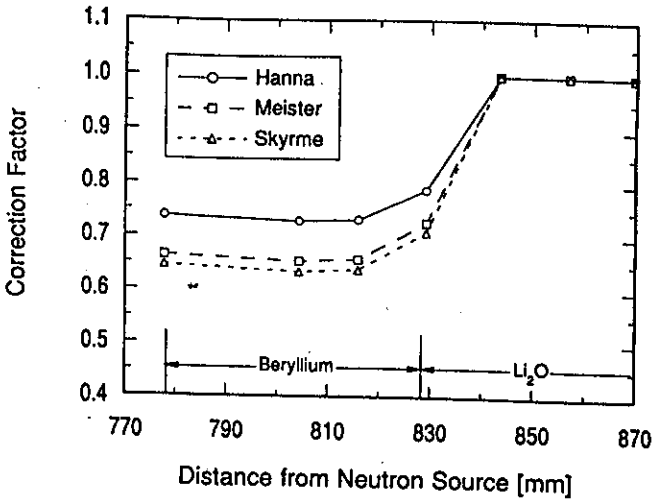

Fig. 13. Self-shielding correction factor for T_6 measurements by the Li-metal foil method for the beryllium front with first-wall (BEFF-B) blanket in Phase-IIB.

In the case of Li-metal, only the self-shielding effect by enriched ^{6}Li became an issue. The self-shielding factor for T_6 measured by enriched ^{6}Li-foil (diameter of 9 mm and thickness of 0.5 mm) in the beryllium front with the first-wall (BEFF-B) blanket of Phase-IIB was estimated[16] by using the neutron spectra calculated by the DOT 5.1 code and the approximate formulas for the self-shielding factor by Hanna,[19] Meister,[20] and Skyrme.[21] The calculated self-shielding correction factor is shown in Fig. 13. This factor was small (large correction) inside the beryllium zone while it is unity behind the beryllium layer. The smallest values occurred in the middle of the beryllium layer, as expected, where the neutron spectrum was the softest.

We conclude that the measured T_6 tends to be smaller than the calculated one in the beryllium zone if the geometrical details of the detector in the calculation model and the self-shielding effect are neglected. Careful attention must be paid to the comparison between the measured and the calculated T_6 inside the beryllium zone in the experimental analysis because the measured T_6 data are not corrected for self-shielding and/or detector void.

IV.C. Comparisons of the Different Techniques for TPR

The TPR was measured by various techniques. The on-line schemes were completely different from the irradiation methods such as the Li-metal foil and the zonal techniques. The consistency of the data obtained from these techniques was examined to ensure the reliability of the measured data.

Figures 14 show the comparisons of TPR of ^{6}Li (T_6) measured with various techniques for REF-A and

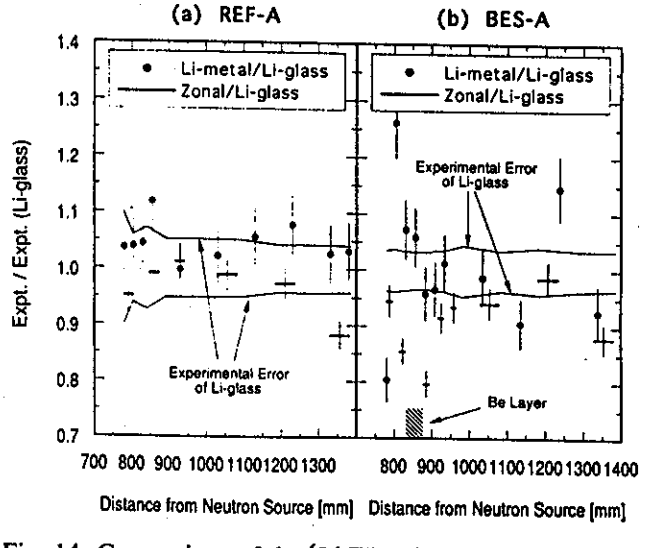

Fig. 14. Comparison of the ^{6}Li TPR data measured by various techniques for (a) the reference (REF-A) and (b) the beryllium sandwiched (BES-A) blanket in Phase-IIA. The relative ratios of TPR measured by the Li-metal foil and the zonal methods to that by the Li-glass method are shown. The horizontal lines stand for the experimental errors of T_6 by Li-glass. The vertical lines are the experimental errors of T_6 by the Li-metal or the zonal method.

BES-A in Phase-IIA. Figure 14 shows relative ratios of T_6 by the Li-metal foil and the zonal methods to that by the Li-glass method. The measured data were not corrected for self-shielding and the flux perturbation by a detector void. Because the agreement between the data was fairly good (within 10%) in REF-A, the tritium measuring technique itself by each method was considered to be consistent. Figure 14b, however, shows that different methods give quite different T_6 data around the beryllium zone. Considering that the zonal method is fundamentally free from such neutron perturbation, we conclude that the T_6 data measured by Li-glass and Li-metal are larger by a few tens of percent around the beryllium layer. This discrepancy was not explained by the detector self-shielding and the neutron perturbation by a detector void because they were large only inside the beryllium zone, as described in Sec. IV.B. The reason for the discrepancy is under investigation.

As for TPR of ^{7}Li (T_7), the same comparisons for REF-A and BES-A are shown in Figs. 15. The relative ratio by T_7 by the Li-metal foil and the zonal methods to that by the Li-glass method are shown in Figs. 15. The NE-213 data were always lower by 15% than the others because the cross-section data [JENDL-3/PR2 (Ref. 11)] of the ^{7}Li$(n,n'\alpha)^3$T used in the data processing of NE-213 were underestimated by ~15% at the 14-MeV region.[22] The data of the Li-metal and the zonal methods were judged to be consistent because their trends were similar. The higher ratios of Li-metal around the beryllium layer in BES-A were probably due to a very small amount of ^{6}Li included in the ^{7}Li-metal foil.

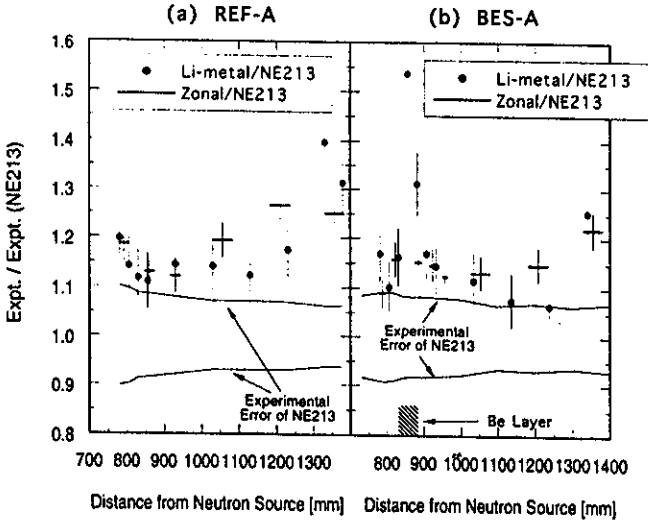

Fig. 15. Comparison of the ^{7}Li TPR data measured by various techniques for (a) the reference (REF-A) and (b) the beryllium sandwiched (BES-A) blanket in Phase-IIA. The relative ratios of TPR measured by the Li-metal foil and the zonal methods to that by the NE-213 method are shown. The horizontal lines stand for the experimental errors of T_7 by NE-213. The vertical lines are the experimental errors of T_7 by the Li-metal or the zonal method.

IV.D. Comparisons of Experimental Data Measured in the Different Systems

The experimental results for various configurations were compared based on those of the reference (REF-A) blanket in Phase-IIA. In the experimental systems, materials such as beryllium and stainless steel were added to REF-A. The ratios of the beryllium front (BEF-A) and beryllium sandwiched (BES-A) blankets in Phase-IIA to REF-A reflected the effect of neutron multiplication in the beryllium layer because the beryllium zone was placed in the front or middle of the Li_2O test zone. As for the reference (REF-B), the beryllium front (BEF-B), and the beryllium front with first-wall (BEFF-B) blankets in Phase-IIB, the beryllium multiplier zone was added to the inner surface of the Li_2CO_3 container with the stainless steel liner. The comparison between REF-A and REF-B led to the effects of neutron reflection in the beryllium liner. The mixed effects of neutron reflection and multiplication by the beryllium were deduced from the ratios of BEF-B and BEFF-B to REF-A.

IV.D.1. TPR

Because the experimental data with Li-glass and NE-213 were available for all experimental assemblies, comparisons of TPR of ^{6}Li (T_6) and ^{7}Li (T_7) were made based on these data.

The change of T_6 and T_7 due to the neutron multiplication by beryllium is compared for Phase-IIA systems in Fig. 16. The T_6 in the beryllium layer was enhanced (a factor of 6 to 7) due to the very soft spectrum inside the beryllium layer. As a result, T_6 at the Li_2O zone adjacent to the beryllium layer became large (a factor of 3 to 4). This enhancement of T_6 decreased at the position deeper than 100 mm behind the beryllium layer probably because low-energy neutrons generated inside the beryllium layer were absorbed rapidly by ^{6}Li of the Li_2O zone. On the other hand, T_7 decreased by 8% in the Li_2O zone behind the beryllium layer.

Figure 17 shows the same ratios of T_6 and T_7 in the Phase-IIB systems. Figure 17 indicates the change of T_6 and T_7 due to the neutron reflection and multiplication by the inner beryllium layer in Phase-IIB. The beryllium liner increased T_6 by a factor of 20 at the front of the test zone and T_7 by 10% over the test zone. The beryllium liner and the beryllium layer in the test region gave a very large increase of T_6 by a factor of 50. The first wall in the front of the test region decreased both T_6 and T_7 by ~10%.

Table IX summarizes the TPR integration along the center axis (line-integration) in the Li_2O zone using T_6

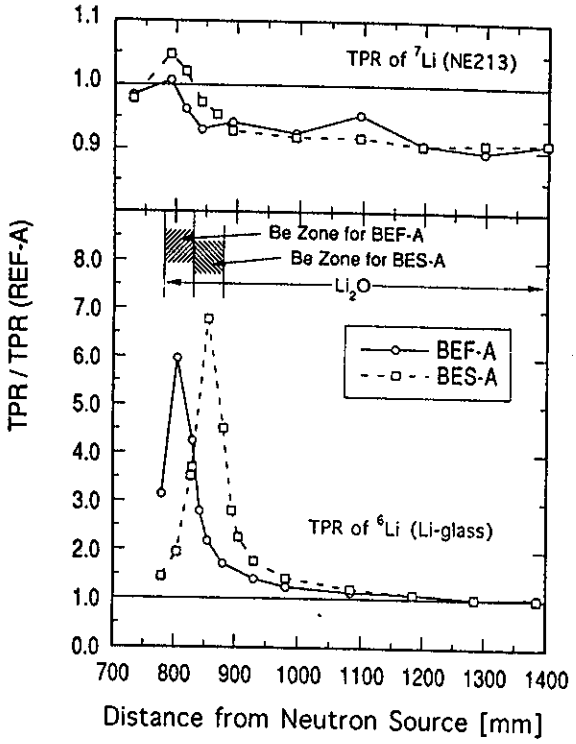

Fig. 16. Comparison of the TPR from ^{6}L (T_6) by Li-glass and ^{7}Li (T_7) by NE-213 for the reference (REF-A), the beryllium front (BEF-A), and the beryllium sandwiched (BES-A) blankets in Phase-IIA. The relative ratios to T_6 and T_7 for REF-A are shown.

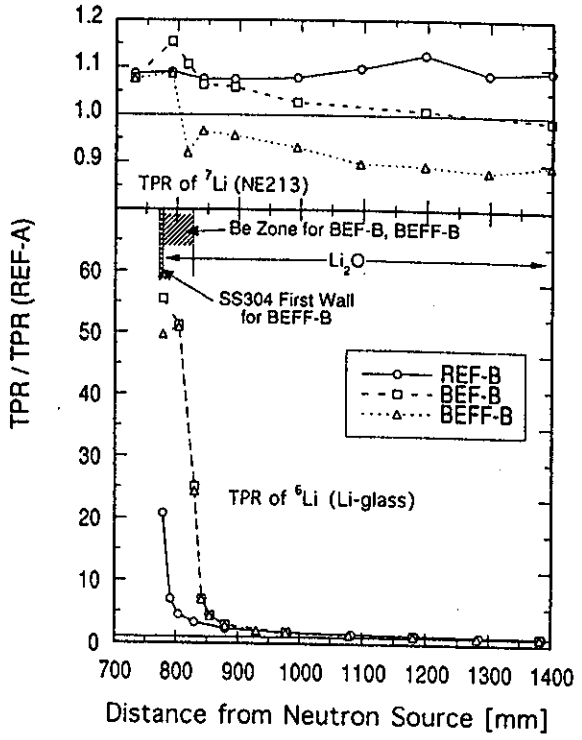

Fig. 17. Comparison of TPR from ^{6}L (T_6) by Li-glass and ^{7}Li (T_7) by NE-213 for the reference (REF-B), the beryllium front (BEF-B), and the beryllium front with first-wall (BEF-B) blankets in Phase-IIB. The relative ratios of T_6 and T_7 for the reference (REF-A) blanket in Phase-IIA are shown.

and T_7 measured by Li-glass and NE-213. The integrated TPRs in Table IX are indicated as ratios of the value for the REF-A system. As for the beryllium front (BEF-A) blanket in Phase-IIA, T_7 decreased by 34% because the Li_2O region in the test zone was thinner by 50.8 mm because the replacement by the beryllium and T_7 became smaller by 10% behind the beryllium layer while T_6 increased by 17%. The T_n for BEF-A unexpectedly became the same as that for REF-A. On the other hand, T_n for the beryllium sandwiched (BES-A) blanket in Phase-IIA was larger by 19% than that for REF-A because the increase of T_6 was much larger and the decrease of the T_7 was smaller than those for BEF-A.

The inner beryllium liner in Phase-IIB increased T_6 by a factor of 2 to 3 and also gave a small increase of T_7 by 10% compared with T_6 and T_7 for the same blanket configurations in Phase-IIA (REF-A and REF-B, and BEF-A and BEF-B). The first wall in the front of the test blanket zone decreased T_6 and T_7 by 4 and 10%, respectively. The increases of T_n for the Phase-IIB systems were much larger than the increases for the Phase-IIA systems, which indicates that the inner beryllium liner was very effective in obtaining the large tritium breeding ratio. Table IX suggests that REF-B was the best configuration for a tritium production gain among the systems studied. The result, however, was for an asymmetrical system different from a sphere or cylinder. Further consideration of the geometrical configuration is necessary to extrapolate these results to more realistic tritium breeding rate estimation.

TABLE IX

Comparison of the Ratios of TPRs Integrated Along the Center Axis in the Li_2O Zone (Li-Glass and NE-213) to the TPRs for the Reference Blanket (REF-A) in Phase-IIA

Experiment	T_7[a]	T_6[a]	T_n[a]
Phase-IIA			
Beryllium front blanket (BEF-A)	0.66	1.17	1.00
Beryllium sandwiched blanket (BES-A)	0.75	1.41	1.19
Phase-IIB			
Reference blanket (REF-B)	1.08	2.69	2.03
Beryllium front blanket (BEF-B)	0.74	2.05	1.61
Beryllium front with first-wall blanket (BEFF-B)	0.67	1.97	1.52

[a] T_7, T_6, and T_n mean TPR of ^{7}Li, ^{6}Li, and ^{nat}Li, respectively.

IV.D.2. Reaction Rates

Figure 18 shows the ratios of the reaction rates of the $^{27}Al(n,\alpha)^{24}Na$ and $^{115}In(n,n')^{115m}In$ reactions for the beryllium sandwiched (BES-A) blanket in Phase-IIA and the beryllium front with first-wall (BEFF-B) blanket in Phase-IIB to the reaction rates for the reference (REF-A) blanket in Phase-IIA. The reaction rate of $^{27}Al(n,\alpha)^{24}Na$ decreased at the Li_2O zone behind the beryllium layer. This trend was almost the same as that of T_7 by NE-213, shown in Figs. 16 and 17. This supported the consistency between the reaction rate of $^{27}Al(n,\alpha)^{24}Na$ and T_7 by NE-213 because the cross-section curves of both reactions were similar. The ratio of BEFF-B to REF-A in $^{115}In(n,n')^{115m}In$ increased by ~20% at the front of the test region because of the large neutron component reflected by the inner beryllium liner. The beryllium inside the Li_2O did not increase the $^{115}In(n,n')^{115m}In$ reaction rate, which was shown by the ratio of BES-A to REF-A being almost unity.

The ratios of the reaction rates of $^{197}Au(n,\gamma)^{198}Au$ for BES-A and BEFF-B to REF-A are plotted in Fig. 19. The enhancement of the reaction rate of $^{197}Au(n,\gamma)^{198}Au$ due to the existence of beryllium is clearly seen. Figure 19 also shows the ratios for T_6 by Li-glass for comparison. The tendency of $^{197}Au(n,\gamma)^{198}Au$ is similar to that of T_6, although T_6 decreases more rapidly than $^{197}Au(n,\gamma)^{198}Au$ behind the beryllium layer. At the rear positions, the ratios of both reactions are the same and equal to unity.

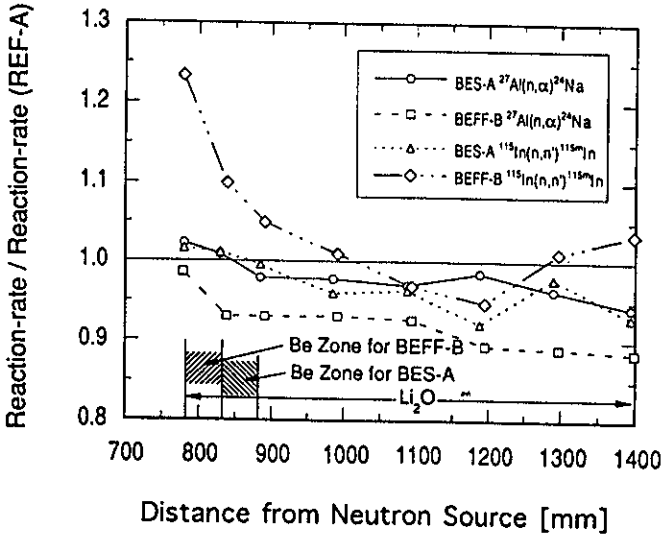

Fig. 18. Comparison of reaction rates of $^{27}Al(n,\alpha)^{24}Na$ and $^{115}In(n,n')^{115m}In$ for the reference (REF-A), the beryllium front (BEF-A) blankets in Phase-IIA, and the beryllium front with first-wall (BEF-B) blanket in Phase-IIB. The relative ratios to the reaction rates for REF-A are shown.

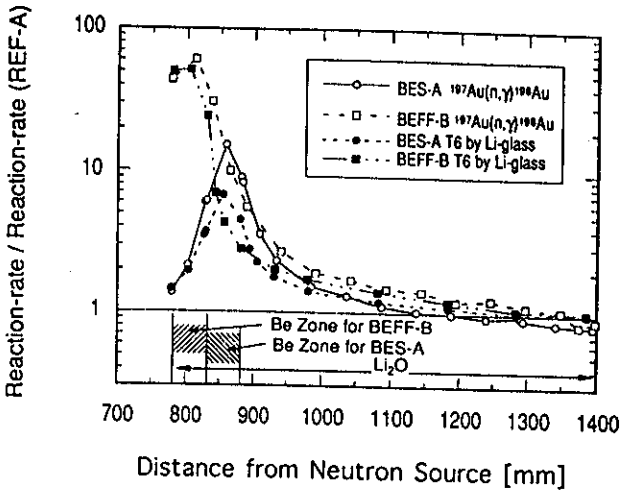

Fig. 19. Comparison of reaction rate of $^{197}Au(n,\gamma)^{198}Au$ for the reference (REF-A), the beryllium front (BEF-A) blankets in Phase-IIA, and the beryllium front with first-wall (BEF-B) blanket in Phase-IIB. The relative ratios to reaction rates in REF-A are shown. The ratios of T_6 measured by Li-glass are also plotted.

IV.E. Comparison with Calculation

The detailed analyses of the experimental data were performed in Refs. 16, 23, and 24. This paper focuses on the analysis that uses the DOT3.5 two-dimensional discrete ordinates code[9] and the FSXJP7 cross-section library[21] (125 groups, P_7) to examine the rough tendency between the measured values and the calculated ones. In FSXJP7, the data for hydrogen, sodium, aluminum, silicon, and calcium were based on JENDL-2 (Ref. 25) while JENDL-3/PR1 (Ref. 10) data were used for chromium, iron, beryllium, oxygen, and nickel. The data for ^6Li, ^7Li, and carbon were extracted from JENDL-3/PR2 (Ref. 11). The first-collision source calculated by the GRTUNCL code was used as an input to DOT3.5. The S_{10} quadrature set was adopted.

Although the whole experimental system was a rectangle shape, it was approximated in a cylindrical model, where each zone volume was conserved. The neutron source was approximated as a point. The room wall and the equipment outside the experimental assembly were not considered because their effects were negligibly small in the center of the Li_2O test region.

The calculated neutron spectra for the beryllium front (BEF-A) blanket in Phase-IIA are already plotted with the measured ones in Fig. 9. The calculation represented very well the measured spectra in energy ranges of above 10 MeV and 10 keV to 1 MeV. The spectra from 2 to 10 MeV were possibly contorted by the insufficient response matrix used in the spectrum unfolding. On the other hand, the discrepancy below 10 keV could be due to the change of the W value, which is the average energy lost by the incident particle per ion pair formed.

Figure 20 compares the measured and the calculated data of the nonthreshold reaction T_6 (TPR of ^{6}Li) and ^{197}Au$(n,\gamma)^{198}$Au for the reference (REF-A), the beryllium sandwiched (BES-A) blankets in Phase-IIA, and the beryllium front with first-wall (BEFF-B) blanket in Phase-IIB. The T_6 measured by Li-glass was used in this comparison. As for T_6, the calculation agreed with the measured values within 10% except around the beryllium regions, where the self-shielding and detector void effects were considered to be the largest. On the contrary, in the ^{197}Au$(n,\gamma)^{198}$Au reaction rate, the agreement was good in the beryllium regions. However, a large discrepancy was observed in the Li_2O region.

The calculated reaction rates of the threshold reaction T_7 (TPR of ^{7}Li) and ^{27}Al$(n,\alpha)^{24}$Na are compared with the measured ones in Fig. 21 for REF-A, BES-A, and BEFF-B. The T_7 data measured by NE-213 were adopted as the measured T_7. Because the same cross section (JENDL-3/PR2) for ^{7}Li$(n,n'\alpha)^3$T was used in the measurement and the calculation, the ambiguity due to the cross-section dose was not in the comparison of T_7. In REF-A, the agreement between the measurement and the calculation was good for both T_7 and ^{27}Al$(n,\alpha)^{24}$Na. On the other hand, the calculation underestimated the measured ^{27}Al$(n,\alpha)^{24}$Na in BES-A and both the measured T_7 and ^{27}Al$(n,\alpha)^{24}$Na in BEFF-B by 10% behind the beryllium layer.

V. CONCLUDING REMARKS

Fusion neutronics experiments were performed on a full-coverage blanket with various configurations of the beryllium neutron multiplier. This experimental system was used to measure nuclear parameters such as TPRs, neutron spectra, and activation reaction rates. The effects of neutron multiplication and reflection by beryllium were examined by using five beryllium configurations.

The TPR was measured by using various techniques such as Li-glass, Li-metal foil, zonal, and NE-213. The measured TPRs of ^{6}Li with these techniques agreed within 10% except for the beryllium zone, where the effects of self-shielding and a detector void were large. The TPRs of ^{7}Li measured by NE-213 were higher by 15% than those measured by the Li-metal and the zonal methods because of the uncertainty of the ^{7}Li$(n,n'\alpha)^3$T cross section from JENDL-3/PR2. The activation reaction rates such as ^{27}Al$(n,\alpha)^{24}$Na, ^{115}In$(n,n')^{115m}$In, ^{197}Au$(n,\gamma)^{198}$Au, etc., were also measured as indices of neutron spectra. The neutron spectrum from a few kilo-electron-volts to 1 MeV and above 2 MeV was measured to provide test data for direct confirmation of neutron transport calculation results.

These measured neutronics parameters were compared among six different configurations of the experimental system. The beryllium layer enhanced T_6 by a

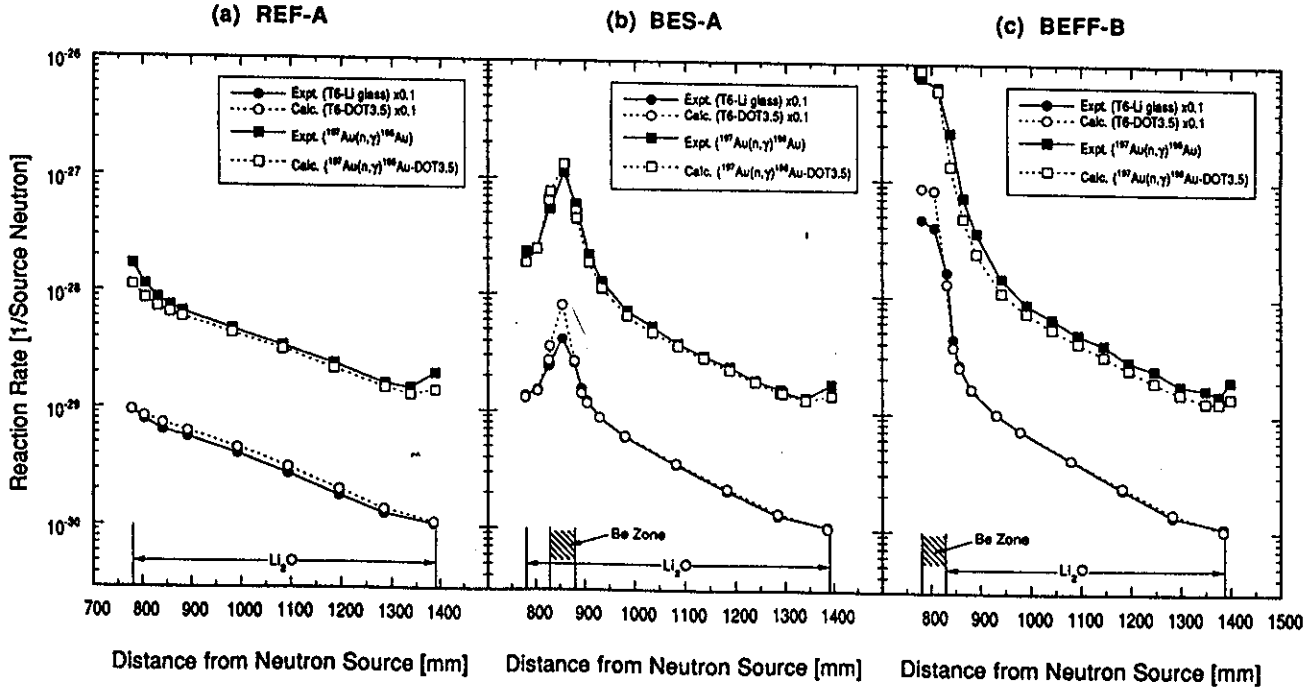

Fig. 20. Comparison of ^{6}Li TPR measured by Li-glass and reaction rate of ^{197}Au$(n,\gamma)^{198}$Au with the DOT3.5 calculation for (a) the reference (REF-A), (b) the beryllium sandwiched (BES-A) blankets in Phase-IIA, and (c) the beryllium front with first-wall (BEFF-B) blanket in Phase-IIB.

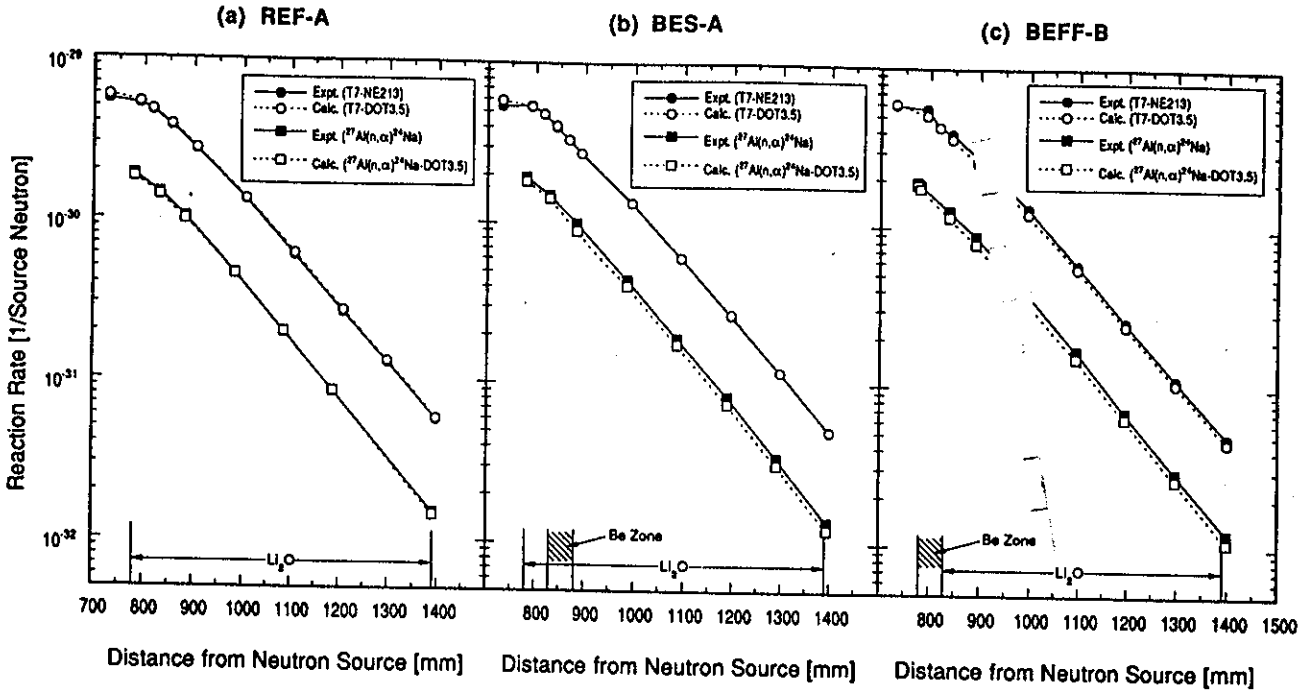

Fig. 21. Comparison of ^{7}Li TPR measured by NE-213 and the reaction rate of $^{27}Al(n,\alpha)^{24}Na$ with the DOT3.5 calculation for (a) the reference (REF-A), (b) the beryllium sandwiched (BES-A) blankets in Phase-IIA, and (c) the beryllium front with first-wall (BEFF-B) blanket in Phase-IIB.

factor of 2 to 5 while it did not affect T_7 much, although a small decrease was seen at the Li_2O zone behind the beryllium layer. The beryllium liner increased T_6 by a factor of 20 at the front of the test zone and T_7 by ~10% over the test zone. Therefore, the blanket configuration with the beryllium liner had great ability for a tritium production gain in the closed geometry. The reaction rates of $^{197}Au(n,\gamma)^{198}Au$ and $^{27}Al(n,\alpha)^{24}Na$ showed the same tendency as T_6 and T_7, respectively.

The calculation by DOT 3.5 using JENDL-3/PR1 and /PR2 agreed with both measured T_6 and T_7 within 10% except for the beryllium zones. The calculation also agreed with the measured activation reaction rates and the neutron spectra.

ACKNOWLEDGMENTS

The authors gratefully acknowledge J. Kusano, C. Kutsukake, S. Tanaka, and Y. Abe for their excellent operation of the FNS accelerator system. The U.S. work was supported by the U.S. DOE Office of Fusion Energy.

REFERENCES

1. M. A. ABDOU, "Tritium Breeding in Fusion Reactors," ANL/FPP/TM-165, Argonne National Laboratory (1982).

2. T. NAKAMURA, H. MAEKAWA, Y. IKEDA, and Y. OYAMA, "A D-T Neutron Source for Fusion Neutronics Experiments at the JAERI," *Proc. 7th Symp. 1983 Int. Ion Sources and Ion-Assisted Technology (ISIAT'83)* and *4th Int. Conf. Ion and Plasma-Assisted Techniques (IPAT'83)*, Kyoto, Japan, September 12-16, 1983, p. 567, Institute of Electrical Engineers of Japan.

3. T. NAKAMURA and M. A. ABDOU, "Summary of Recent Results from the JAERI/U.S. Fusion Neutronics Phase I Experiments," *Fusion Technol.*, **10**, 541 (1986).

4. H. MAEKAWA et al., "Measured Neutron Parameters for Phase I Experiments at the FNS Facility," *Fusion Technol.*, **10**, 564 (1986).

5. S. YAMAGUCHI et al., "An On-Line Method for Tritium Production Measurement with a Pair of Lithium-Glass Scintillators," *Nucl. Instrum. Methods*, **A254**, 413 (1987).

6. Y. OYAMA et al., "A Small Spherical NE213 Scintillation Detector for Use in In-Assembly Fast Neutron Spectrum Measurements," *Nucl. Instrum. Methods*, **A256**, 333 (1987).

7. Y. OYAMA et al., "Phase IIA and IIB Experiments of JAERI/USDOE Collaborative Program on Fusion Blanket Neutronics," JAERI-M 89-215, Japan Atomic Energy Research Institute (1989).

8. M. NAKAGAWA et al., "Characteristics of a Deuterium-Tritium Fusion Source on a Rotating Target Used in Simulated Fusion Blanket Experiments," *Fusion Technol.*, **28**, 39 (1995).

9. W. A. RHOADES and F. R. MYNATT, "The DOT-III Two Dimensional Discrete Ordinates Transport Codes," ORNL-TM-4280, Oak Ridge National Laboratory (1973).

10. K. SHIBATA, "Evaluation of Neutron Nuclear Data of ^{6}Li for JENDL-3," JAERI-M 84-198, "Evaluation of Neutron Nuclear Data of ^{7}Li for JENDL-3," JAERI-M 84-204, and "Evaluation of Neutron Nuclear Data of ^{9}Be for JENDL-3," JAERI-M 84-226, Japan Atomic Energy Research Institute.

11. S. CHIBA, "Revision of the Neutron Nuclear Data of Lithium," *Proc. Specialists Mtg. Nuclear Data for Fusion Neutronics*, JAERI-M 86-029, 32-40, Japan Atomic Energy Research Institute (1986).

12. H. MAEKAWA et al., "Neutron Yield Monitors for the Fusion Neutronics Source (FNS)," JAERI-M 84-193, Japan Atomic Energy Research Institute (1984).

13. M. NAKAZAWA et al., "JENDL Dosimetry File," JAERI 1325, Japan Atomic Energy Research Institute (1992).

14. "FORIST Spectra Unfolding Code," PSY-92, Radiation Shielding Information Center, Oak Ridge National Laboratory (1975).

15. E. F. BENNETT and T. J. YULE, "Techniques and Analyses of Fast Reactor Neutron Spectroscopy with Proton-Recoil Proportional Counters," ANL-7763, Argonne National Laboratory (1971).

16. M. Z. YOUSSEF et al., "US/JAERI Collaborative Program on Fusion Neutronics, Phase IIA and IIB Fusion Integral Experiments, the US Analysis," UCLA-ENG-90-14, University of California, Los Angeles (1990).

17. W. A. RHOADES, Oak Ridge National Laboratory, Private Communication (1987).

18. R. A. MacFARLANE, "TRANSX-CTR: A Code for Interfacing MATXS Cross-Section, Libraries to Nuclear Transport Codes for Fusion Systems Analysis," LA-9863-MS, Los Alamos National Laboratory (1984).

19. G. C. HANNA, "The Neutron Flux Perturbation Due to an Absorbing Foil; A Comparison of Theories and Experiments," *Nucl. Sci. Eng.*, **15**, 325 (1963).

20. H. MEISTER, "Aktivierungsstörung von Indiumfolien im Neutronenfeld," *Z. Naturforsch A*, **10**, 669 (1955).

21. T. H. R. SKYRME, MS-91 and MS-91A, 2nd ed., Atomic Energy Research Establishment (1944).

22. M. NAKAGAWA et al., "US/JAERI Collaborative Program on Fusion Neutronics, Phase I Fusion Integral Experiments, Volume II: Analysis," JAERI-M 88-177, Japan Atomic Energy Research Institute (1988).

23. M. NAKAGAWA et al., "JAERI/US Collaborative Program on Fusion Blanket Neutronics—Analysis of Phase IIA and IIB Experiments," JAERI-M 89-154, Japan Atomic Energy Research Institute (1989).

24. M. Z. YOUSSEF et al., "Nuclear Analysis of Integral Experiments on a Li_2O Test Assembly with Local Heterogeneities Utilizing a 14-MeV Neutron Source," *Fusion Technol.*, **28**, 243 (1995).

25. "Summary of JENDL-2 General Purpose File," JAERI-M 84-103, T. NAKAGAWA, Ed., Japan Atomic Energy Research Institute (1984).

Chikara Konno (MS, physics, Kyoto University, Japan, 1985) is a research scientist in the Department of Reactor Engineering at the Japan Atomic Energy Research Institute (JAERI). He has worked in the areas of fusion neutronics experiments, cross-section measurements, and neutron spectrum measurements using a proton-recoil counter.

Yukio Oyama (BS, physics, 1975; MS, nuclear physics, 1977; and Dr. Eng., 1989, Osaka University, Japan) is a principal scientist at JAERI. He has worked in the area of fusion neutronics experiments since 1978. He is currently involved in intense and high-energy neutron source projects.

Yujiro Ikeda (PhD, nuclear engineering, Nagoya University, Japan, 1981) is head of the Fusion Neutronics Laboratory in the Department of Reactor Engineering at JAERI. He has worked in the areas of fusion neutronics experiments, induced radioactivity experiment and analysis, direct nuclear heating measurements, activation cross-section measurements, and fusion dosimetry.

Seiya Yamaguchi (BS, applied physics, Waseda University, Japan, 1980; MS, 1982, and PhD, 1989, energy sciences, Tokyo Institute of Technology, Japan) in 1982 joined the Department of Reactor Engineering at JAERI, where he engaged in research and development on the design and characterization of Li-glass scintillator for fusion neutronics application. From 1989, he was a research assistant with Photon Factory at KEK, National Laboratory for High Energy Physics, where he worked in the areas of microwave engineering for the electron linear accelerator.

Koichi Tsuda (BS, nuclear engineering, University of Tokyo, Japan, 1982) is a research scientist at JAERI. He has worked in the area of fusion neutronics experiments since 1982. He is especially involved in tritium measurement.

Kazuaki Kosako (BE, atomic engineering, Tokai University, Japan, 1984) has worked at Sumitomo Atomic Energy Industries since 1994. He worked in the Department of Reactor Engineering at JAERI from 1984 to 1992 where he was involved mainly in fusion neutronics. He is currently interested in the area of radiation damage of materials.

Hiroshi Maekawa (BE, 1965; MS, 1967; and Dr. Eng., 1970, nuclear engineering, Tokyo Institute of Technology, Japan) is the deputy director of the Department of Reactor Engineering and the head of the Intense Neutron Source Laboratory at JAERI. He has worked on fusion neutronics for more than 20 years, and he planned and constructed the Fusion Neutronics Source facility. He served as the Japanese leader of the JAERI/U.S. Department of Energy (U.S. DOE) collaboration on fusion blanket neutronics. His recent research has focused on International Fusion Materials Irradiation Facility conceptual design activities.

Masayuki Nakagawa (BS, 1965; MS, 1967; and PhD, 1979, nuclear engineering, Kyoto University, Japan) is a principal scientist in the Department of Reactor Engineering at JAERI. He is a head of the reactor system laboratory having the main responsibility for the computation method and design of reactors. He researched the development of neutronics computation methods and codes for fast reactors and fusion reactors and intelligent reactor design systems. His group has developed high-speed general-purpose Monte Carlo codes based on vector and/or parallel algorithms.

Takamasa Mori (BS, 1976; MS, 1979; and PhD, 1985, nuclear engineering, Kyoto University, Japan) is a principal scientist in the Department of Reactor Engineering at JAERI. He worked for the development of neutron transport codes using double-differential form cross sections. His research interests are in the field of reactor physics, especially the speedup of Monte Carlo calculation of high-energy particles based on vector and/or parallel algorithms.

Tomoo Nakamura (BS, physics, Kyoto University, Japan, 1957) is currently director of the Public Acceptance Database Center, Research Organization for Information Science and Technology. His research background includes experimental reactor physics on fast breeder reactors and nuclear technology on fusion reactor blankets. He served as the former Japanese leader of the JAERI/U.S. DOE collaboration on fusion blanket neutronics.

Mohamed A. Abdou is a professor in the Department of Mechanical, Aerospace, and Nuclear Engineering at the University of California, Los Angeles (UCLA) and also is the director of fusion technology at UCLA. His research interests include neutronics, thermomechanics, fusion technology, and reactor design and analysis. He served as the U.S. leader of the JAERI/U.S. DOE collaboration on fusion blanket neutronics.

Edgar F. Bennett (PhD, University of New Hampshire, 1957) is a physicist at Argonne National Laboratory (ANL). He has been a section head of experimental reactor physics since 1970. He is best known as the inventor of a widely used in-core proton-recoil spectrometer—a technique that he has been continually updating. He has also made contributions to the field of reactivity measurement by reactor noise techniques, in particular, by providing a common theoretical basis and introducing a new type of variance experiment.

Karl Gustav Porges (PhD, University of California, Berkeley, 1952) is currently retired. He was a research physicist at ANL from 1958 through 1990. Areas of special interest to him include nuclear reactions, fission, neutron physics, nuclear reactor safety, mechanical and electronics instruments design, probability and stochastic theory, fluid mechanics, fusion blanket design, and tritium chemistry.

Mahmoud Z. Youssef-(PhD, nuclear engineering, University of Wisconsin, 1980) is a senior research engineer in the Department of Mechanical, Aerospace, and Nuclear Engineering at UCLA. He participated in several conceptual magnetic fusion energy and inertial fusion energy reactor design studies with emphasis on nuclear analysis and blanket/shield design. His research interests are in the areas of blanket/shield design optimization, nuclear data, sensitivity/uncertainty studies, neutronics methods and code development, tritium fuel cycle, radioactivity and safety aspects of fusion, integral experiments, neutronics testing, and research and development for fusion reactors, particularly the International Thermonuclear Experimental Reactor (ITER).